SATIF-15:
15th Workshop on Shielding aspects of Accelerators, Targets, and Irradiation Facilities

Facility for Rare Isotope Beams (FRIB) at Michigan State University
East Lansing, Michigan USA
20-23 September 2022.

Session 5: Code Benchmarking & Intercomparison (continuation) / Induced Radioactivity & Decommissioning

Table of contents

Session 5: Code Benchmarking & Intercomparison (continuation) / Induced Radioactivity & Decommissioning 1

1. Overview of benchmark studies at the CERN Shielding Benchmark Facility (CSBF) and the CERN High Energy Accelerator Mixed Field (CHARM) facility in the CERN East Experimental Area 3
Robert Froeschl, Davide Bozzato, Markus Brugger, Arnaud Devienne, Angelo Infantino, Tsuyoshi Kajimoto, Vasiliki Kouskoura, Eunji Lee, Noriaki Nakao, Takahiro Oyama, Stefan Roesler, Toshiya Sanami

2. Radiation protection aspects of Long Shutdown 3 at the CERN LHC experiments: a methodology for residual activation assessments applied to the CMS case study 13
Tommaso Lorenzon, Davide Bozzato, Robert Froeschl, Vasiliki Kouskoura

3. Activation calculations of selected RPV internal components for optimal decommissioning of nuclear power plants 23
Reuven Rachamin, Jörg Konheiser, Marcus Seidl

4. Radiation protection studies for new beam dumps at ISOLDE at CERN 33
Alice Formento, Elodie Aubert, Ana-Paula Bernardes, Alexandre Dorsival, Jose Maria Martin Ruiz, Stefano Marzari, Simon Mataguez, Eliseo Perez-Duenas, Fabio Pozzi, Heinz Vincke, Joachim Vollaire

5. Activation benchmarking of metals by 9.6 GeV electrons at PAL-XFEL 44
Nam-Suk Jung, Mahdi Bakhtiari, UkJae Lee, Hee Hoon Kim, Hee-Seock Lee

6. Radiation transport calculations supporting the ISIS muon collimator replacement project . 45
Steven Lilley

1. Overview of benchmark studies at the CERN Shielding Benchmark Facility (CSBF) and the CERN High Energy Accelerator Mixed Field (CHARM) facility in the CERN East Experimental Area

Robert Froeschl[1*], Davide Bozzato[1,2], Markus Brugger[1], Arnaud Devienne[1], Angelo Infantino[1], Tsuyoshi Kajimoto[3], Vasiliki Kouskoura[1], Eunji Lee[4], Noriaki Nakao[5], Takahiro Oyama[4], Stefan Roesler[1], Toshiya Sanami[4]

[1]CERN, European Organization for Nuclear Research, 1211 Geneva 23, Switzerland
[2]Karlsruher Institut für Technologie (KIT), Kaiserstraße 12, 76131 Karlsruhe, Germany
[3]Hiroshima University, 1-4-1, Kagamiyama, Higashi-Hiroshima, Hiroshima 739-8527, Japan
[4]High Energy Accelerator Research Organization (KEK), 1-1, Oho, Tsukuba, Ibaraki 305-0801 Japan
[5]Institute of Technology, Shimizu Corporation, 3-4-7, Etchujima, Koto-ku, Tokyo 135-8530, Japan

[*]robert.froeschl@cern.ch

The CERN High Energy AcceleRator Mixed Field (CHARM) Facility is situated in the CERN Proton Synchrotron (PS) East Experimental Area. The facility receives a pulsed proton beam from the CERN PS with a beam momentum of 24 GeV/c with 5e11 protons per pulse with a pulse length of 350 ms and with a maximum average beam intensity of 6.7e10 protons per second. The extracted proton beam impacts on a cylindrical target, made of copper or aluminium.

The shielding of the CHARM facility includes the CERN Shielding Benchmark Facility (CSBF) situated laterally above the target that allows deep shielding penetration benchmark studies of various shielding materials. This facility has been significantly upgraded during the extended technical stop at the beginning of 2016.

One week of beam time at the CHARM facility is typically allocated during a normal operational year for radiation benchmark studies. This paper presents an overview of benchmarks for Monte Carlo radiation simulation transport codes performed with data from the CSBF and the CHARM facilities over the last years. This includes a series of benchmarks for activation inside the CHARM target room, in the shielding structure of the CSBF as well as in the access maze of the CHARM facility. These benchmarks cover high energy neutron reactions, low energy neutron activation and activation in mixed fields and have been performed with the FLUKA and PHITS Monte Carlo codes. Several active measurements will be discussed, including neutron spectra measurements using NE213 scintillators and Bonner spheres as well as ambient dose equivalent measurements.

The CSBF and CHARM facilities are very versatile with ample benchmark potential still to be explored. Lessons learnt from the previous measurement campaigns and ideas for future benchmark experiments at the CSBF and CHARM facilities are finally presented.

1.1. Introduction

The CERN High Energy AcceleRator Mixed Field (CHARM) Facility is situated in the CERN Proton Synchrotron (PS) East Experimental Area. The CHARM facility has been constructed in 2013-14 together with the IRRAD facility that is located directly upstream of the CHARM facility. The purpose of the CHARM facility is to create mixed radiation fields in which electronic components and entire systems can be tested for radiation effects.

During the construction of the CHARM facility, a prototype of the CERN Shielding Benchmark Facility (CSBF) has been incorporated in the roof shielding of the CHARM

facility directly laterally above the target. Based on the operational experience in 2015, the CSBF has been significantly upgraded in the Year-End Technical Stop of 2015/16. The purpose of the CSBF is to study deep shielding penetration radiation fields.

The CHARM and CSBF are very well suited for benchmark experiments because of the well-known geometrical configuration, beam parameters than can be varied over a wide range and very good beam and radiation instrumentation.

In this contribution, several benchmark experiments and their comparison to Monte Carlo code predictions are presented after a brief description of the facilities themselves. This includes measurements inside the CHARM facility itself, at the CSBF prototype in 2015 and at the upgrade CSBF in the years from 2016 to 2018.

1.2. Description of CHARM

Figure 1.1 presents a sketch of the layout of the CHARM facility. The radiation protection assessment of the CHARM facility can be found in (Froeschl, 2014) and the commissioning results are documented in (Froeschl, 2016).

Figure 1.1. Layout of the CHARM facility

Note: View at beam height level. The CSBF is located laterally above the Target location.
Source: Froeschl, Brugger, Roesler (2014)

The CHARM facility receives a pulsed proton beam that is slowly extracted from the CERN PS with a pulse length of 350 ms. It has a beam momentum of 24 GeV/c with 5e11 protons per pulse and with a maximum average beam intensity of 6.7e10 protons per second. This assumes 6 cycles (i.e. 6 pulses) within a super-cycle of the CERN PS of 45.6 seconds. The extracted proton beam impacts on a cylindrical target, made of copper or aluminium.

The beam intensity send to the CHARM facility can be changed in several ways. Using a dedicated low-intensity slow extraction, the number of protons per pulse can be reduced from 5e11 down to 3e9 with several intermediate steps. Furthermore, the number of cycles per super-cycle can be varied, typically from 1 to 6 cycles for an average CERN PS super-cycle of 45.6 seconds.

In addition to the variation of the beam intensity sent to CHARM, the strength of the radiation fields generated by the interaction of the proton beam with the target can be varied

by a factor of 9 by exchanging the Copper target with an Aluminium target with slits (to reduce the effective density). A full solid Aluminium target can also be used as an intermediate step. All target exchanges can be performed fully remotely within less than 1 minute.

The beam intensity sent to the IRRAD and CHARM facilities is monitored with a secondary emission chamber with a systematic uncertainty of ~5%. The statistical uncertainty on the beam intensity for typical benchmark experiments is far below the systematic one.

One week of beam time at the CHARM facility is typically allocated during a normal operational year for radiation benchmark studies. The benchmark experiments presented in this study have been performed during these dedicated weeks in the years 2015 to 2018.

1.3. Benchmarks inside the CHARM facility

A series of benchmarks was conducted for the radiation fields inside the CHARM facility to probe the understanding of the source term for the radiation in the CHARM target room and, consequently, the radiation in the access maze and the shielding structures.

The knowledge of thermal neutron fluences inside accelerator installations is important for the prediction of the production rates of ^{41}Ar since it significantly contributes to the radioactivity concentration in the exhaust air after a cool-down time of one hour. Gold foils were used inside the CHARM target room to measure the thermal neutron fluxes. The reaction rates for bare gold foils and Cadmium coated gold foils were measured and then compared to predictions from the MARS, PHITS and FLUKA codes (Oyama, 2018). The agreement between Monte Carlo simulations and the measured values is better than a factor of 2.

The yields of secondary particles from targets, notably the yield of neutrons, as a function of the angle with respect to the axis of the impinging beam is an important ingredient for the design of shielding structures. The high-energy components of these secondary particles from a dedicated Copper target were measured in CHARM using activation detector sets, each consisting of aluminum, niobium, indium, and bismuth disks, at 30 cm placed around the target at angles from 15° to 160°. The production rates of several reaction channels were then compared with predictions from FLUKA simulations (Oyama, 2021). The setup and the production rate comparison are shown in Figure 1.2. FLUKA simulations allowed to understand the contribution of charged hadrons and photons to several production rates. The agreement between Monte Carlo simulations and the measured values is better than a factor of 2.

The radiation streaming through the access maze of the CHARM facility has been characterized in (Nakao, 2021). Ten aluminium detectors have been placed in the access maze and the ^{24}Na production rates have been measured by gamma spectrometry and then compared to predictions of the PHITS and FLUKA codes. The setup and the result of the comparison are presented in Figure 1.3. The calculated rates by PHITS and FLUKA generally are in good agreement with each other. The calculated rates agree with the experiment within 30% in Leg-1 and Leg-2 of the maze. Then, the difference becomes larger in Leg-3 and further along the maze where the worst agreement is a factor of 1.7. This is a remarkable agreement since the production rates vary over more than 3 orders of magnitude.

Figure 1.2. Activation experiment at various angles for a Copper target and comparison to FLUKA simulations.

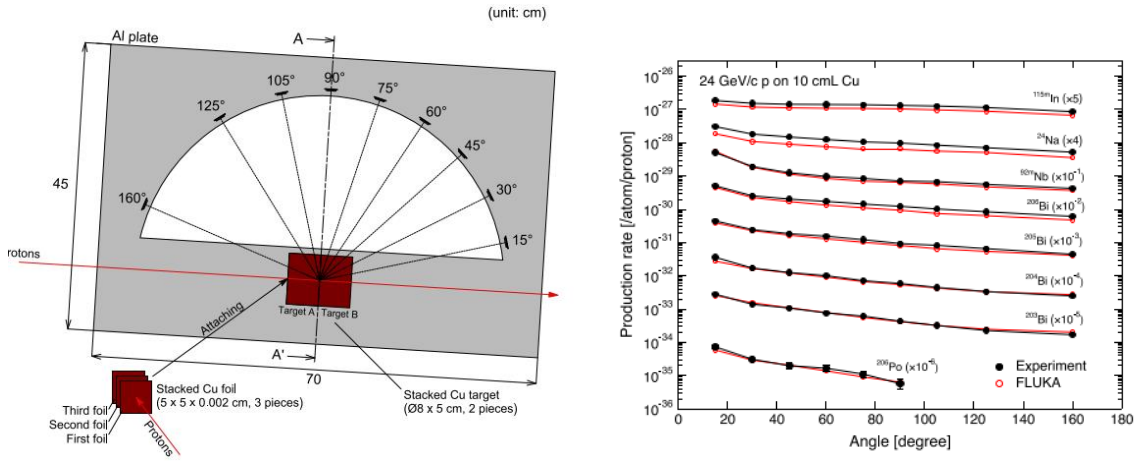

Source: Oyama (2021)

Figure 1.3. Setup of activation experiment in CHARM access maze and comparison to PHITS and FLUKA Monte Carlo simulations

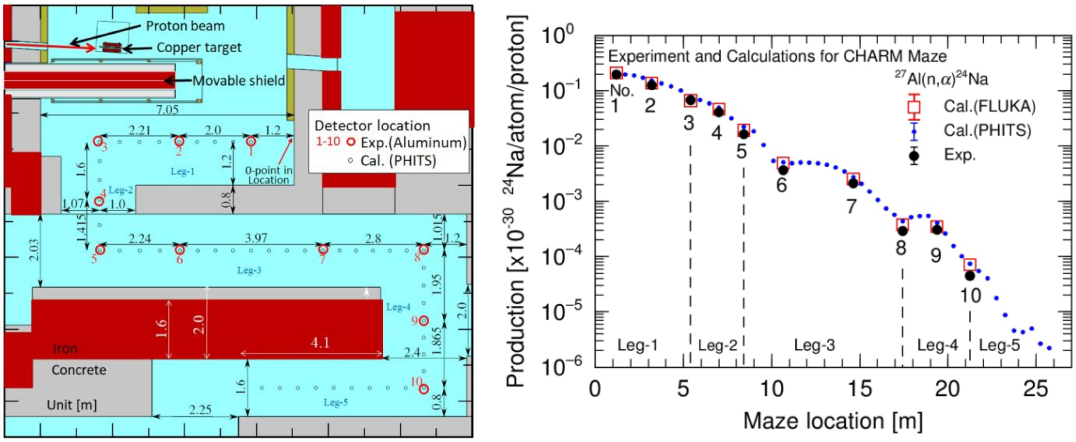

Source: Nakao (2021)

A benchmark using active detectors focusing on the radiation effects to electronic components inside the CHARM target room has been performed in (Prelipcean, 2022). The agreement between the measured values of the radiation monitors employed and prediction by the FLUKA code is on average around ±20% for Beam Loss Monitors, Optical Fibre sensors, radio-photoluminescence glass dosimeters, and radiation monitors measurements of the Total Ionizing Dose and high-energy hadron fluence. An overestimation by approximately a factor of 2 is observed in the case of thermal neutron fluence measurements.

1.4. Benchmark experiments at the CSBF prototype in 2015

During the construction of the CHARM facility in 2014, a first prototype of the CERN Shielding Benchmark Facility (CSBF) has been integrated in the CHARM shielding laterally above the CHARM target. Figure 1.4 presents the layout of the prototype of the CSBF during operation in the year 2015. The purpose of the CSBF is to perform benchmarks in deep shielding penetration neutron radiation fields.

Figure 1.4. Layout of the prototype of the CSBF in the year 2015

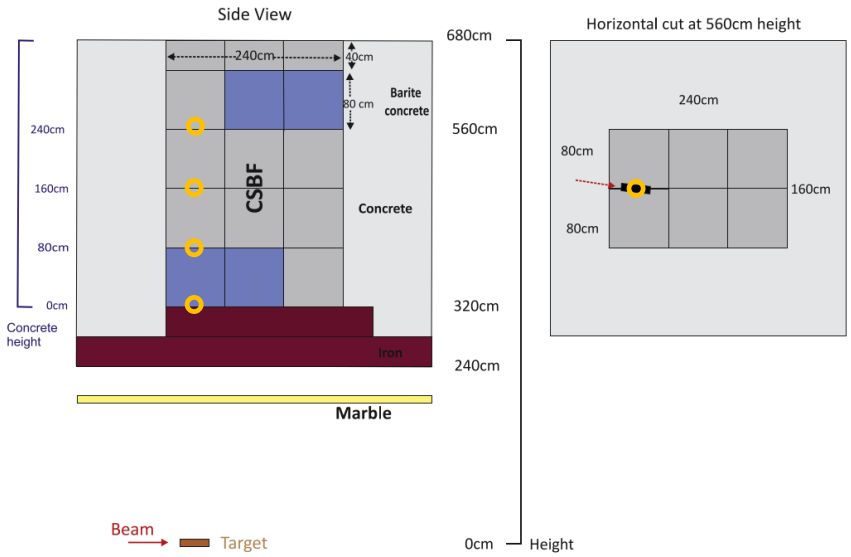

Note: The four locations of activation samples are indicated by the orange circles.
Source: Iliopoulou (2018, Nucl.Instrum.Meth.A)

Activation samples of bismuth and aluminium are very well suited to measure high-energy neutrons and therefore have been placed in 2015 at four locations in the CSBF prototype and in the CHARM target room. The measured production rates of several bismuth isotopes and ^{24}Na have been compared with prediction from FLUKA simulations (Iliopoulou, 2018, Nucl.Instrum.Meth.A). The agreement between FLUKA Monte Carlo simulations and the measured production rates is better than a factor of 2 in all cases (see Figure 1.5).

The activation sample technique has then also been used to experimentally determine the attenuation length of high energy neutrons in these shielding materials (Nakao, 2020). The experimentally obtained attenuation length for concrete is 120 ±7.0 g/cm^2. This value is consistent with previous measurements.

The neutron energy spectrum has been measured using an NE213 scintillator on top of the CSBF roof (Kajimoto 2018). The NE213 scintillator was used as the neutron detector because it provides the neutron spectrum in the energy range from several MeV up to a few hundred MeV. Due to the spill structure (300 ms duration), the time-of-flight technique cannot be used in this configuration. Therefore, an unfolding technique using an iterative Bayesian algorithm was applied to obtain the neutron energy spectrum on the CSBF roof.

Figure 1.5. Comparison of production yields at the CSBF prototype

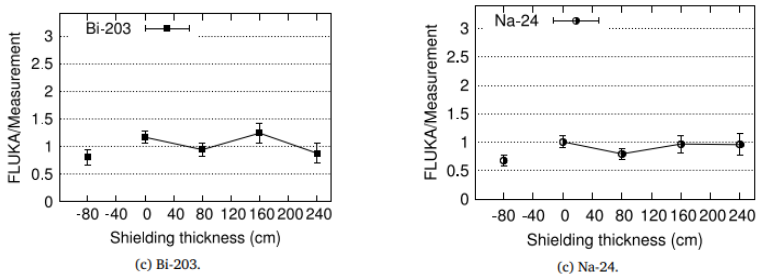

Note: Location -80 refers to a location inside the CHARM target room
Source: Iliopoulou (2018, Nucl.Instrum.Meth.A)

1.5. Benchmark experiments at the upgraded CSBF

Based on the experience collected during the operation of the CSBF in 2015, an upgrade of the CSBF has been performed in the Year-End Technical Stop 2015/16. The layout of the upgraded CSBF during normal beam operation is shown in Figure 1.6.

The shielding structure of the CSBF consists of 40 cm of cast iron and up to 400 cm of concrete. The concrete structure comprises a 200 cm long removable sample holder concrete block with 4 locations for activation samples, a material test location for the measurement of the attenuation properties of shielding materials as well as a dedicated platform for measurements in deep penetration neutron fields.

Activation campaigns using bismuth, aluminium, indium and carbon samples have been performed in 2016 and 2017 at the upgraded CSBF. The measured production rates have been compared to the estimated production rates from FLUKA Monte Carlo simulations (Iliopoulou, 2018, 2021). The agreement is at a level of a factor of 2 (see Figure 1.7).

Figure 1.6. Layout of the upgraded CSBF since 2016

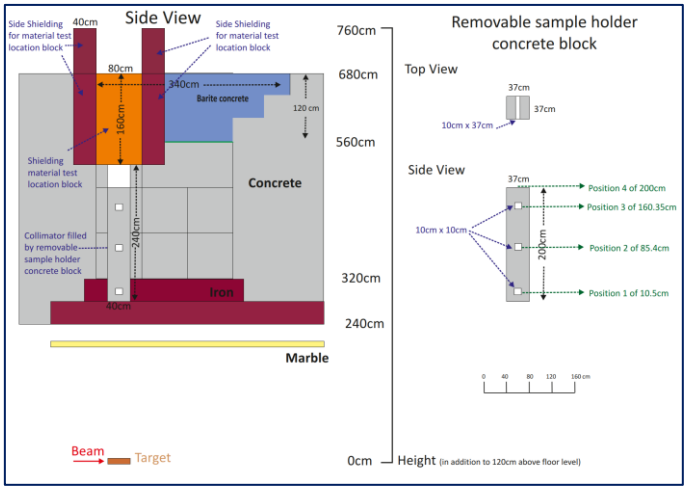

Source: Iliopoulou (2018)

Figure 1.7. Comparison of production yields at the upgraded CSBF

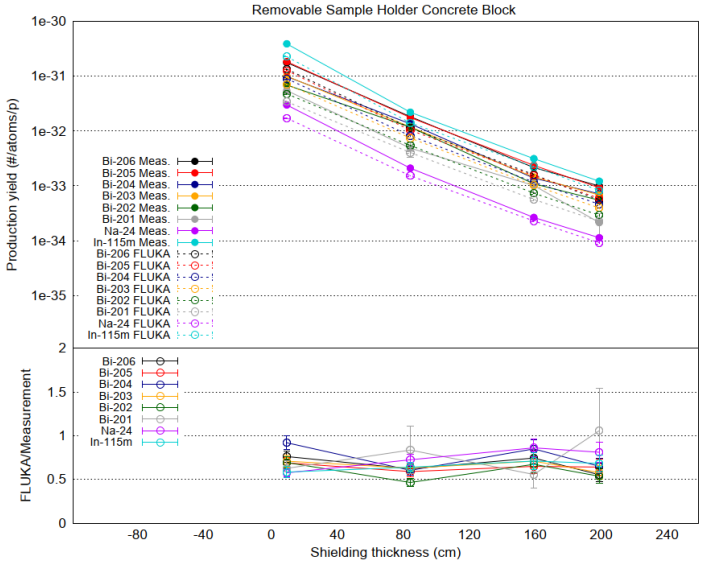

Source: Iliopoulou (2018)

Experimental measurements of the spectra of neutrons after the penetration of concrete and steel shielding of various thicknesses have been performed at the CSBF using an NE213 scintillator (Lee, 2021). The thicknesses of concrete and steel ranged up to 360 cm and 80 cm, respectively. The various configurations are presented in Figure 1.8.

Charged particle events were removed via plastic veto scintillators and photons via pulse shape discrimination. The neutron energy spectra have then been obtained by unfolding the light output distributions from the NE213 scintillator using the response functions calculated with the SCINFUL-QMD code (Satoh, 2002).

The measured neutron spectra are shown in Figure 1.9 together with the comparison to the spectra estimated by PHITS Monte Carlo code simulations. The agreement of the measurements with the PHITS estimates was within a factor of 1.5 for energies from 20 MeV to 150 MeV and closer to a factor for 2 for energies above 150 MeV.

The measured spectra have then been used to calculate the attenuation lengths for the shielding materials. The results of the attenuation lengths were consistent with previous results obtained by activation detectors.

1.6. Summary and Conclusions

The CHARM and the CSBF facilities are located in the CERN PS East Experimental Area and use the radiation fields generated by a pulsed proton beam with a beam momentum of 24 GeV/c with 5e11 protons per pulse with a pulse length of 350 ms impacting on a target in the CHARM facility.

State-of-the-art beam and radiation instrumentation as well as a wide tuning range of the beam intensity make the CHARM and CSBF very good facilities for benchmark experiments. An overview of the benchmark experiments, focusing on neutron fields, performed in recent years at these facilities has been presented in this study. From a general perspective, the agreement between the measured neutron field quantities and Monte Carlo

code predictions is typically within a factor of 1.5 inside the CHARM target chamber and within a factor of 2 in the shielding structures that were up to 360cm thick, notable for the PHITS and FLUKA Monte Carlo simulation codes.

The experience gained from performing these benchmark experiments has been used to design the next set of benchmark measurement campaigns. These comprise active measurements using Rem-Counters, Bonner Spheres Spectrometers and ionization chambers with well-known response functions as well as passive measurements using activation detectors, notably in forward direction, and CR-39 dosemeters.

Figure 1.8. Measurement configurations for neutron spectra measurements using an NE213 scintillator

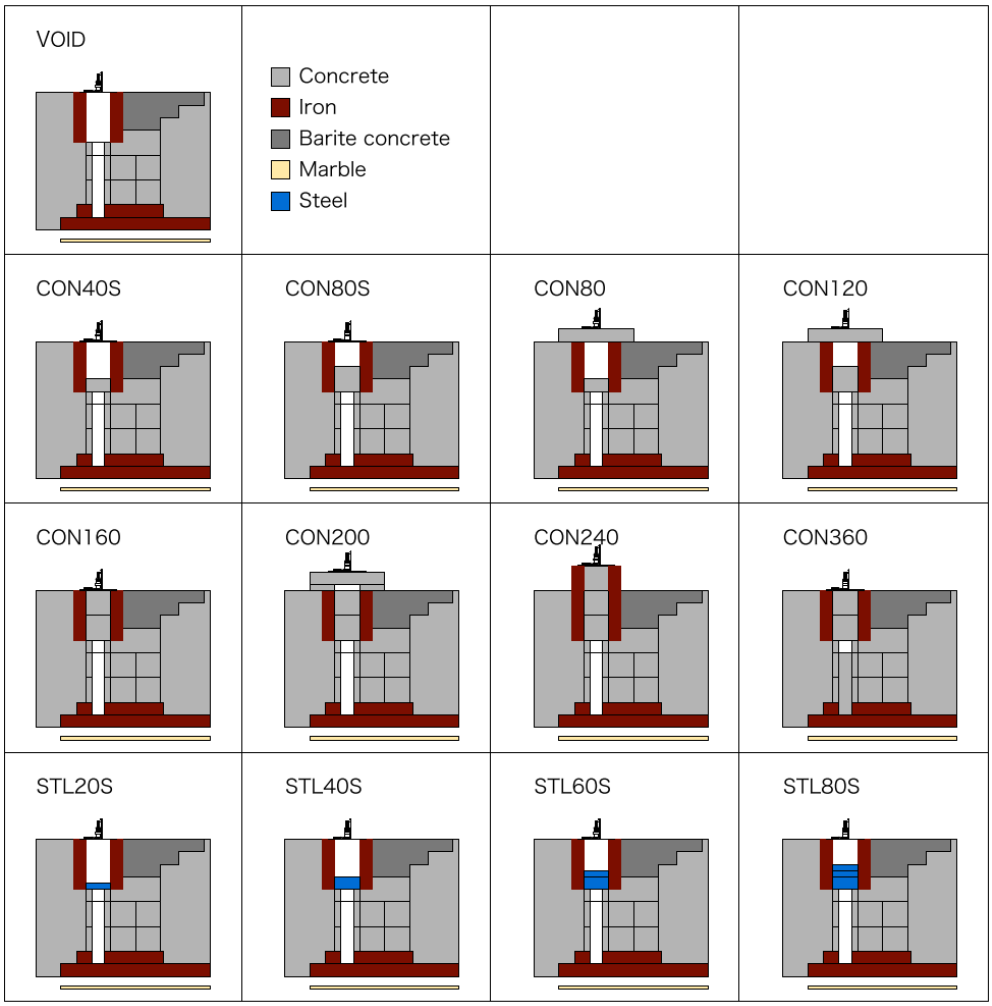

Note: Only the shielding structure of the CSBF laterally above the CHARM target is shown. The principle layout including the CHARM target is shown in Figure 1.6.
Source Lee (2021)

Figure 1.9. Comparison of neutron spectra measured using an NE213 scintillator for various shielding materials and thicknesses to PHITS Monte Carlo simulations

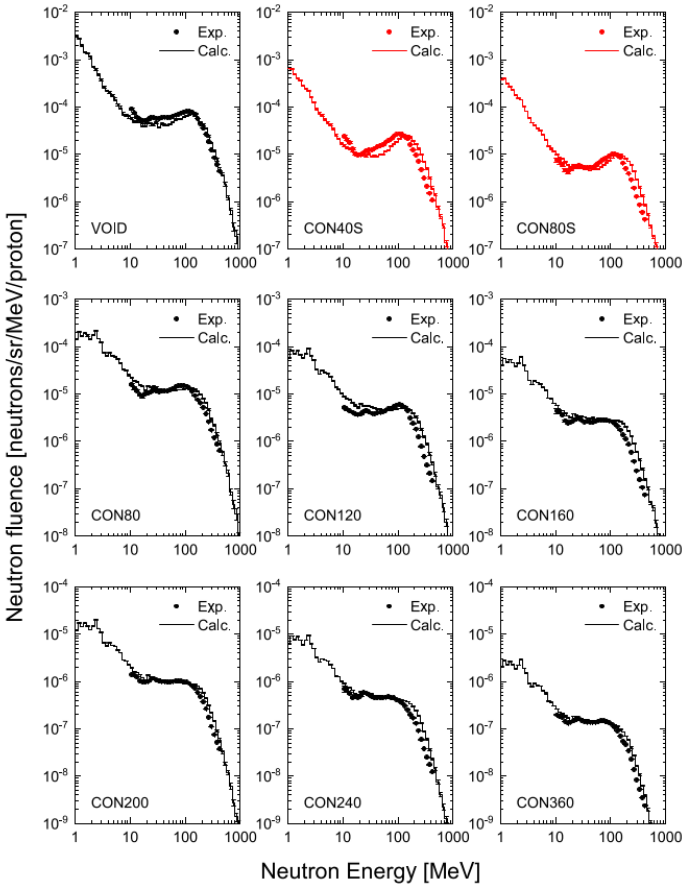

Note: The corresponding shielding configurations can be found in Figure 1.8.
Source: Lee (2021)

1.7. List of references

Froeschl, R., Brugger, M. and Roesler, S. (2014), "The CERN High Energy Accelerator Mixed Field (CHARM) facility in the CERN PS East Experimental Area", Proceedings of SATIF12, NEA/NSC/R(2015)3, Batavia, Illinois, United States, p. 14-25.

Froeschl, R. et al. (2016), "Radiation Protection Aspects of the Commissioning and Operation of the CERN High Energy Accelerator Mixed Field (CHARM) facility in the CERN East Experimental Area", Proceedings of SATIF 13 NEA/NSC/R(2018)2, Dresden, Germany, p. 163-171.

Iliopoulou, E. et al. (2018), "Measurements and FLUKA Simulations of Bismuth, Aluminium and Indium Activation at the upgraded CERN Shielding Benchmark Facility (CSBF)", J.Phys.Conf.Ser. 1046 (2018) 1, 012004, DOI:10.1088/1742-6596/1046/1/012004.

Iliopoulou, E. et al. (2018), "Measurements and FLUKA simulations of bismuth and aluminium activation at the CERN Shielding Benchmark Facility (CSBF)", Nucl.Instrum.Meth.A 885 (2018) 79-85, DOI:10.1016/j.nima.2017.12.058.

Iliopoulou, E. et al (2021), "Measurements and FLUKA simulations of bismuth, aluminium, indium and carbon activation at the upgraded CERN Shielding Benchmark

Facility (CSBF)", Proceedings of SATIF 14 NEA/NSC/R(2021)2, Gyeongju, Korea, p. 250-266.

Kajimoto, T. et al. (2018), "Neutron energy spectrum measurement using an NE213 scintillator at CHARM", Nucl.Instrum.Meth.B 429 (2018) 27-33, DOI:10.1016/j.nimb.2018.05.024.

Lee, E. et al. (2021), "Energy spectra of neutrons penetrating concrete and steel shielding blocks from 24 GeV/c protons incident on thick copper target", Nucl.Instrum.Meth.A 998 (2021) 165189, DOI:10.1016/j.nima.2021.165189.

Nakao et al. (2020), "Attenuation length of high energy neutrons through a thick concrete shield measured by activation detectors at CHARM", J.Nucl.Sci.Tech. 57 (2020) 9, 1022-1034, DOI:10.1080/00223131.2020.1751740

Nakao, N. et al. (2021), "Measurements and Monte Carlo simulations of high-energy neutron streaming through the access maze using activation detectors at 24 GeV/c proton beam facility of CERN/CHARM", J.Nucl.Sci.Tech. 58 (2021) 8, 899-907, DOI:10.1080/00223131.2021.1887003.

Oyama, T. et al (2018), "Measurement and calculation of thermal neutrons induced by the 24 GeV/c/c proton bombardment of a thick copper target", Nucl.Instrum.Meth.B 434 (2018) 29-36, DOI:10.1016/j.nimb.2018.08.016.

Oyama, T. et al (2021), "Measurements of secondary-particle emissions from copper target bombarded with 24-GeV/c protons", Nucl.Instrum.Meth.A 990 (2021) 164977, DOI:10.1016/j.nima.2020.164977.

Prelipcean, D. et al (2022), "Benchmark Between Measured and Simulated Radiation Level Data at the Mixed-Field CHARM Facility at CERN", IEEE TRANSACTIONS ON NUCLEAR SCIENCE, VOL. 69, NO. 7, JULY 2022, DOI:10.1109/TNS.2022.3169756.

Satoh, D. et al. (2002), "Development of SCINFUL-QMD code to calculate the neutron detection efficiencies for liquid organic scintillator up to 3 GeV", J. Nucl. Sci. Technol. 39 (2002) 657–660, DOI:10.1080/00223131.2002.10875185.

1.8. List of abbreviations and acronyms

BLM	Beam Loss Monitor
CERN PS	CERN Proton Synchrotron
CHARM	CERN High Energy AcceleRator Mixed Field
CSBF	CERN Shielding Benchmark Facility
IRRAD	IRRADiation proton facility

2. Radiation protection aspects of Long Shutdown 3 at the CERN LHC experiments: a methodology for residual activation assessments applied to the CMS case study

Tommaso Lorenzon[1*], Davide Bozzato [1,2], Robert Froeschl [1], Vasiliki Kouskoura [1]
[1]CERN, European Organization for Nuclear Research, 1211 Geneva 23, Switzerland
[2]Karlsruher Institut für Technologie (KIT), Kaiserstraße 12, 76131 Karlsruhe, Germany
[*]tommaso.lorenzon@cern.ch

The Large Hadron Collider (LHC) at CERN is currently in the early stages of Run 3, i.e. the third operational period of its lifecycle during which the machine will provide particle collisions to the four experiments located along the accelerating ring. Starting from the end of 2025, a three-year Long Shutdown (LS) period, denoted as LS3, will follow. The upgrade work foreseen during this stop represents an essential milestone for the LHC, bringing it to the second phase of its physics programme (High Luminosity LHC, HL-LHC).

To fully exploit the HL-LHC increased delivered luminosity, the LHC experiments have scheduled major upgrades to their detectors. Among the others, this is the case for the Compact Muon Solenoid (CMS), which has planned the installation of new components, as well as the dismantling of some others. This process is organised according to a complex work plan, during which the CMS configuration is sequentially modified over time to make accessible its various parts, including the innermost areas of the detector. In such a complex scenario, the radiological impact of the activated components must be assessed.

This paper focuses on the preparation of a Long Shutdown inside the LHC experiments from an operational radiation protection viewpoint, presenting CMS as a case study. In particular, the computational methodology developed at CERN to assess the residual ambient dose equivalent rates inside the experimental caverns based on the FLUKA Monte Carlo code is discussed.

First, LHC Run 3 operational parameters are addressed, as well as the computational tools required for the analysis. Afterwards, focusing on the CMS case study, the pipeline of configurations foreseen for LS3 is illustrated. Eventually, the most representative results of this assessment are presented and briefly discussed. These will provide the CMS collaboration with useful data to organise LS3 following a dose optimization approach.

2.1. Introduction

The Large Hadron Collider (LHC) at CERN is currently the largest particle accelerator in the world. It can accelerate protons, as well as fully stripped lead ions $^{208}Pb^{82+}$, and provide collisions (proton-proton, $^{208}Pb^{82+}$-$^{208}Pb^{82+}$, proton-$^{208}Pb^{82+}$) at four locations around its ring (Evans and Bryant, 2008). At these interaction points, the so-called *large experiments* (ALICE, ATLAS, CMS, LHCb) are installed below ground to record the LHC high-energy particle collisions using their unique detectors.

The LHC programme is based on a highly organised timeline that alternates periods (about three years long) of physics operations (Runs) run as well as Long Shutdowns (LS); in addition, 2-3 short technical stops of 1 week are usually planned in an operation year. While during Runs the machine is fully operational and the beams are circulating in the accelerator to achieve collisions, Long Shutdowns are scheduled to access the experimental caverns and intervene on the machines. Technical stops are reserved for maintenance along the year.

Long Shutdowns are crucial for the advancement of the LHC physics programme and represent a considerable challenge in terms of planning. In fact, inside the experimental caverns, maintenance and complex interventions on the large experiments are planned. In an enormous collaborative effort, structures and sub-detectors can undergo several inspections, upgrades, complete substitutions; new components may be installed, while others may leave the detector for being dismantled. This process is organised according to an elaborated work plan, during which the detector configuration is sequentially modified over time to make accessible its various parts, including its innermost areas.

Currently, the LHC is in the early stages of Run 3, i.e. the third period of beam time in the machine since the beginning of operations in 2011. Run 3 is planned to last until the end of 2025, providing proton-proton collisions at the record energy of $\sqrt{s}$ = 13.6 TeV and a levelled luminosity of 2×10^{34} cm^{-2} s^{-1} (Bozzato et al., 2022). By the end of 2025, and starting from year 2026, LS3 will follow. Starting from Run 4 and after a consistent upgrade, the LHC will enter in the second phase of its lifecycle, the so called High-Luminosity LHC (HL-LHC). The HL-LHC project will ensure the full exploitation of the LHC potential (Brüning and Rossi, 2015); the upgraded machine is expected to integrate ten times more luminosity than the LHC, posing significant challenges for radiation tolerance and event pileup on detectors, especially for calorimetry in the forward region. To withstand these new operation conditions, in particular the increased delivered luminosity, the large experiments have scheduled major upgrades to their detectors. Most of the interventions are planned for the LS3, which will clearly be of crucial importance for the LHC physics programme.

From an operational radiation protection viewpoint, the prompt radiological impact caused by a typical LHC run is minimal. In fact, most of the accelerator infrastructure is located underground (LHC lies below ground at a depth approximately between 45 m and 170 m). This, together with a strict control on access procedures, minimizes the risk of external exposure. On the other hand, Long Shutdowns present a completely different radiological scenario. Secondaries from the high-energy collisions contribute to create a unique field of prompt radiation, which is responsible for the activation in detectors and infrastructure materials. Therefore, for all the LS-related activities, such as handling of activated equipment, the risk of external exposure due to decay radiation (mostly gamma radiation) must be assessed.

In this situation, it is natural to conclude that activation and residual ambient dose equivalent rate calculations are indispensable for LS-related activities. Preliminary studies are usually carried out already during the design phase and assessments are required for optimizing and establishing protection measures in planned exposure situations (Work Dose Planning) with an ALARA approach, for the radiological classification of areas, for the characterization of radioactive components for their elimination pathway or transport, and in general to ensure an efficient operational radiation protection.

2.2. Computational approach

Long Shutdown activation and residual dose rate computations at LHC large experiments present a major challenge, which is the need to reproduce and model the changes that detectors undergo in their configuration between runs and shutdowns. In fact, the nominal position in which structures and devices might get activated during a Run could be different from the one where they are stored, or simply moved, during a Long Shutdown.

Figure 2.1. Two-steps simulations diagram for LS-related activities

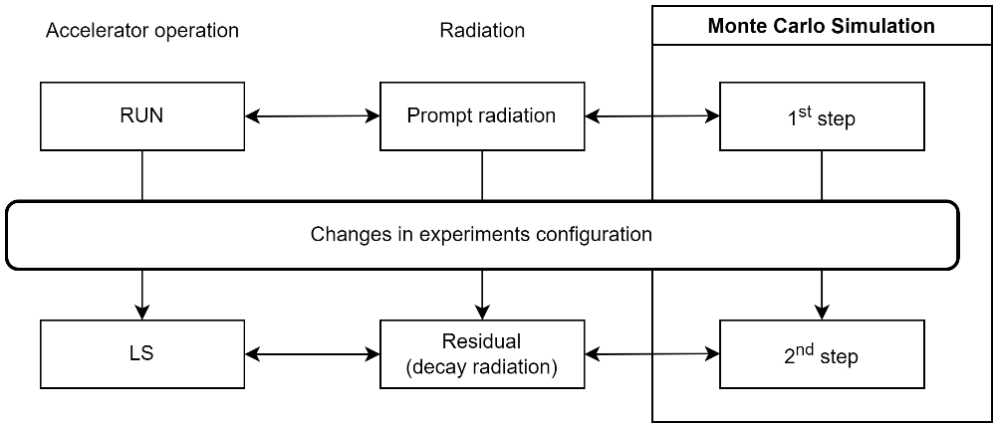

Two steps simulations for LS-related activities at the CERN LHC. The large experiments undergo substantial modifications in their configuration during Long Shutdowns. Dose rate evaluations for Long Shutdowns must take this into account. Simulations are split into two steps, corresponding to the LHC Run, responsible of activating environment and equipment, and the Long Shutdown, during which the residual activation decays.

2.2.1. FLUKA

Traditionally, activation and residual dose rate evaluations are performed with a Monte Carlo transport code. At CERN, the general-purpose Monte Carlo code FLUKA is used (Ahdida et al., 2022; Battistoni et al, 2015; FLUKA.CERN, 2022). FLUKA is an extremely powerful tool able to provide residual dose rates estimates, but with some limitations. Firstly, only one irradiation profile per simulation can be considered; secondly, the flexibility for simulating residual transport radiation is limited to possibly activate/deactivate the electromagnetic fields and change regions material, *de facto* allowing to model only the removal of objects from a geometry (if the material is set to air).

The essential requirement of reproducing the evolution of an experimental cavern configuration inside FLUKA translates into the need of assessing the activation in the Run (nominal) configuration, and to score residual dose rates from activated components after having modelled their movements in space. Also, it might be desired to suppress in-air radioactivity contributions: this is an effective solution to consider the air recirculation that is put in place during maintenance works inside the caverns.

At CERN, the most up-to-date methodology used by the Radiation Protection (RP) group to carry out these evaluations is to split simulations into two steps (Figure 2.1), with the support of the SESAME code.

2.2.2. SESAME

SESAME (Cooijmans and Guthoff, 2015; Froeschl, 2020) provides the workflow and a set of tools that allow to effectively split prompt and decay transport for complex two-steps simulations. Also, it allows to easily introduce FLUKA geometry transformations between the two steps.

SESAME was originally developed by the CMS collaboration and is currently maintained by the CERN RP group. It is written in Python 3 and C++ and is strongly coupled to FLUKA through few custom Fortran routines. Thanks to this interconnection, SESAME does not interfere with any FLUKA feature; therefore, the Monte Carlo code is not subject to any limitation and also advanced simulation techniques such as biasing can still be put in place.

Figure 2.2. SESAME workflow for a two-steps FLUKA simulation

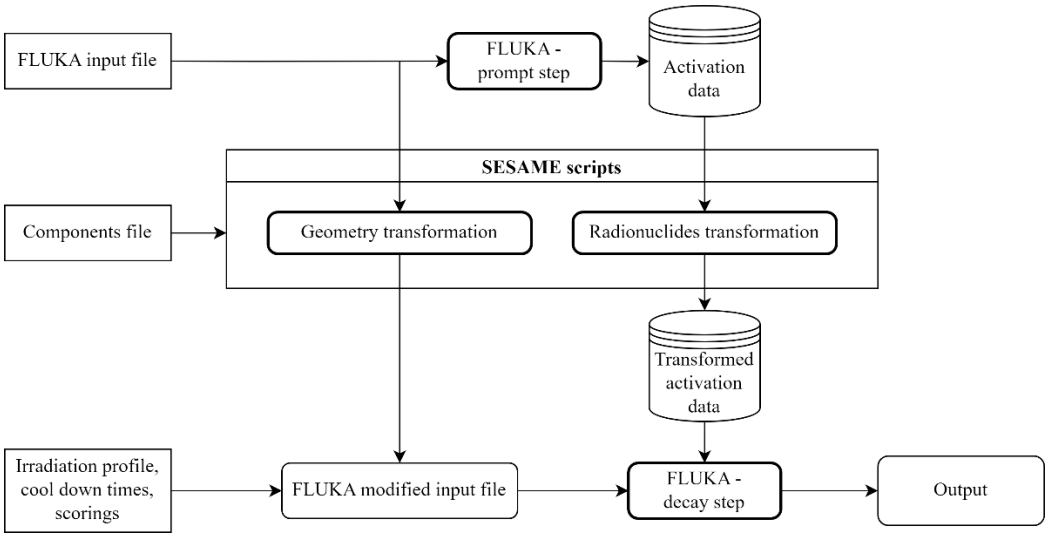

Diagram of the typical workflow adopted for two-steps residual dose rates simulations at the CERN LHC. A more complete version of the diagram, including SESAME advanced features and routines description, is available in (Froeschl, 2020).

First step

In the first step, the FLUKA simulation of the primary process of interest is performed. At this stage, the only interface between FLUKA and SESAME is a set of custom FLUKA routines that dumps all the information regarding activation produced during the prompt simulation (unstable radionuclide creation events) to binary files. The following data is stored: index of the prompt primary that produced the nuclide, atomic number, mass number, isomeric state, spatial location (x, y, z), statistical weight, index of the FLUKA region in which the nuclide was produced.

Second step

The second step allows the user to introduce geometrical transformations in the input file and to perform a FLUKA simulation for the decay of the various radionuclides produced in the first step.

The geometry transformation is accomplished by providing SESAME with a simple text file (in jargon called *component file*) containing a list of directives organised in a specific syntax. Directives are applied to components, defined as a set of FLUKA regions that are to be treated identically (in other words, a component is a *union* of regions). Typically, the regions are adjacent, and the component corresponds to a composite object (e.g. a sub-module of a detector). Currently, it is possible to describe multiple roto-translations and command the deactivation or removal of a component from space. SESAME autonomously generate a new FLUKA input file that includes the transformations requested (Figure 2.2).

This file requires a manual clean-up. Provided that the geometry transformations were correctly defined, fixes are generally required to redefine air regions that might come in conflict with moved components or might be left empty by the component transformations themselves. Also, all the transformations that cannot be expressed in the component file have to be introduced manually at this point of the workflow. This is the typical case of the installation of a new shielding in the considered geometry.

Figure 2.3. CMS detector

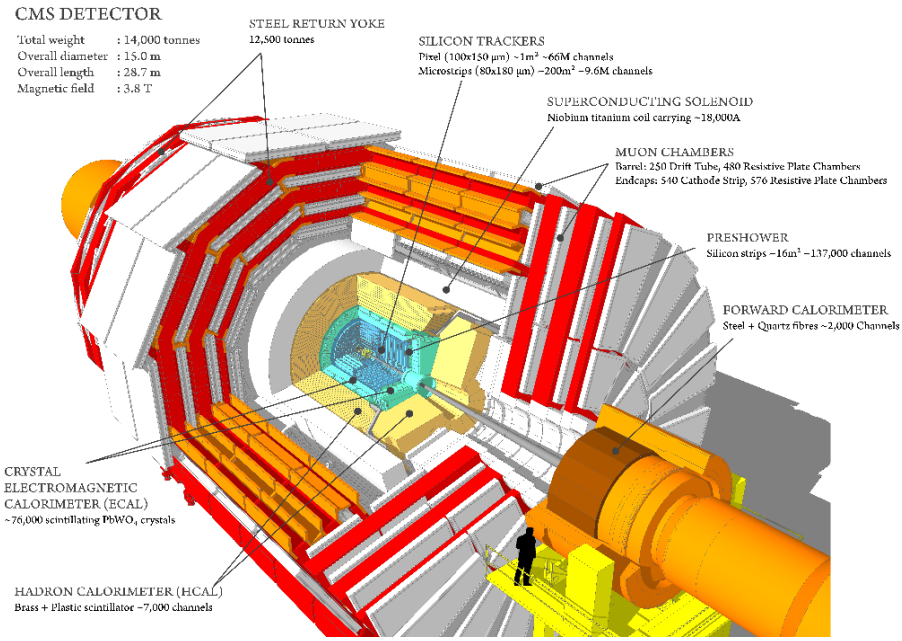

Schematic of the CMS detector. CMS is a general-purpose detector located about 100 m underground close to the French village of Cessy, between the Lake of Geneva and the Jura mountains. Copyright CERN. Source: CERN Document Server, https://cds.cern.ch

Starting from the same component file, a C++ program takes care of propagating the indicated geometric transformation to the radionuclide inventory stored from the first step. This means that the activity scored in the prompt step is moved accordingly to the component in which it was produced. To make sure that the geometry and nuclide transformations correspond, a Python script is available to inspect the distribution of the resulting nuclides.

The simulation of the decay step consists of a FLUKA run in which the prompt activity, after being transformed, is loaded and made to decay in the newly created geometry. Before submitting the second step, an irradiation profile, decay times and associated scorers should be added, like in any other activation simulation. In practice, a custom FLUKA executable defines a source routine that loads the decay nuclides as primary particles for FLUKA to simulate. In this sense, the second step should be intended as a fully independent activation simulation; therefore, further features can be added with respect to the prompt step, such as biasing.

2.3. CMS case study

As mentioned, at one of the four collision points along the LHC, the Compact Muon Solenoid (CMS) is installed. CMS is a general-purpose detector, i.e. it was designed to observe any new physics phenomena that the LHC might reveal (The CMS Collaboration, 2008).

CMS is located about 100 m underground close to the French village of Cessy, between the Lake of Geneva and the Jura mountains. The overall dimensions of the detector are a length of 21.6 m, a diameter of 14.6 m and a total weight of 14000 t (Figure 2.3). The CMS detector is shaped like a cylindrical onion, with several concentric layers of components, including a 6-m-inner-diameter, 4-T superconducting solenoid, muon chambers, silicon trackers, barrel and forward calorimeters (hadron and electromagnetic).

Figure 2.4. Two different CMS detector configurations

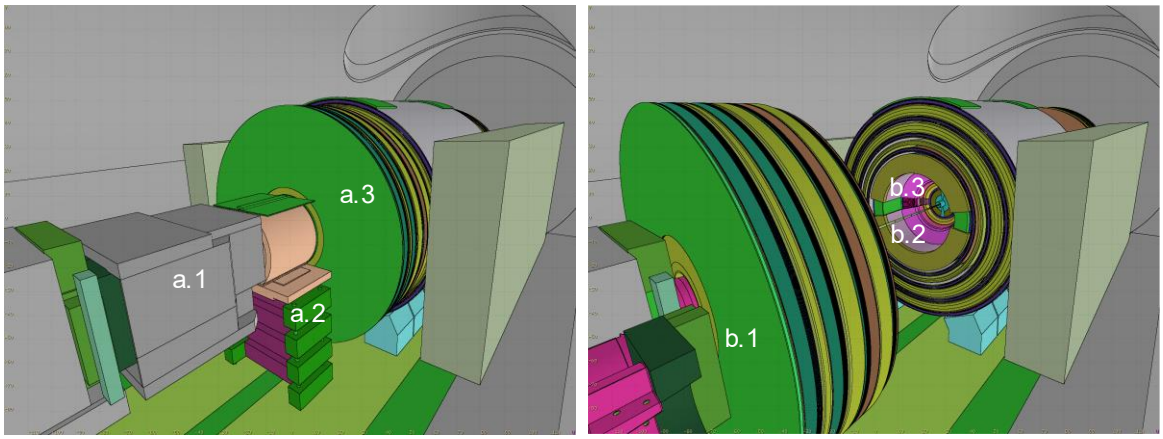

Two different CMS configurations, as implemented in FLUKA and visualised with Flair 3D viewer (Vlachoudis, 2009). On the left, CMS in the nominal configuration (a). On the right, CMS in the "open disk" scenario (b), realized with SESAME and a specific component file. More details about the components tagged in the picture can be found in the text.

2.3.1. LS3 DR simulation

A preliminary work plan for LS3 at CMS was made available to the CERN RP group for evaluating residual dose rates in the experimental cavern. The pipeline for the LS-related activities was subdivided in 10 different detector configurations, also referred to as *scenarios*. These include the nominal (closed) configuration, the opening of the CMS forward shielding (known as Rotating Shielding), the successive removal of the Hadron Forward calorimeters and opening of the endcap disks, and finally the sequential removal of the inner systems, such as the beam pipe, the tracking detectors, and the electromagnetic and hadron calorimeters.

Based on the approach that was previously presented, the simulation workflow consisted of:

1. One prompt simulation, with proton-proton collisions at $\sqrt{s}$ = 14 TeV; this beam energy slightly overestimates of few percents the design one for conservative purposes.
2. A decay step simulation for each configuration; a component file was manually prepared for each scenario to transform the nominal prompt geometry by applying the SESAME scripts.

Figure 2.4 shows a 3D view of the CMS detector model, as implemented in FLUKA. In picture 2.4 (a), the CMS nominal configuration (closed detector) is reproduced. Among the various components, it is possible to observe the forward shielding elements (a.1), the hadronic forward calorimeter and its support riser (a.2), and the last endcap disk (a.3). Figure 2.4 (b) shows the geometry of the "open disk" scenario, obtained by transforming the nominal geometry using SESAME and a dedicated component file corresponding to this configuration. After removing and opening the forward shield elements and the hadronic forward calorimeters and opening the endcap disk (b.1), it is possible to access the beam pipe (b.2) and the inner tracking systems of the detector (b.3).

Figure 2.5. CMS nominal configuration; residual ambient dose equivalent rate map at 1 month of cool down time after the end of proton-proton operations before LS3

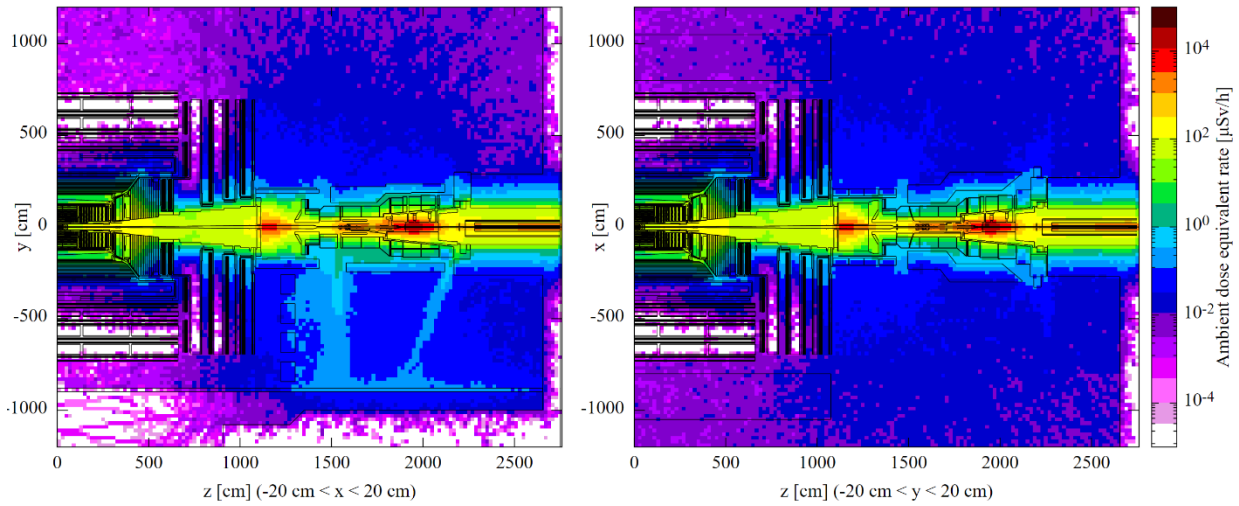

Residual ambient dose equivalent rate maps after 1 month cool down time after the end of proton-proton operations before the beginning of LS3; CMS in closed configuration. Vertical (left) and horizontal (right) cuts of the CMS experimental cavern.

For the second step, an irradiation profile for Run 3 had to be assumed. In fact, while the irradiation history up to LS2 is known, the future performance of LHC and the delivered luminosity can inevitably only be hypothesized. For RP predictive studies, the estimation of the irradiation profile is obtained evaluating an average luminosity delivered during an operational year (Bozzato et al., 2022). This depends on the levelled luminosity and on the global machine availability. With this information, the irradiation time is then computed as the number of seconds required to reach a target integrated luminosity within one calendar year. The computed irradiation time is eventually placed as one single period of continuous irradiation at the end of the year. For this study, it was conservatively assumed that the integrated luminosity per calendar year in Run 3 is 35 fb^{-1}, 90 fb^{-1}, 90 fb^{-1}, 90 $fb^{-}1$ for years 2022, 2023, 2024 and 2025 respectively, while the levelled luminosity is assumed to be 2 × 10^{34} $cm^{-2}s^{-1}$ for all the four years (Bozzato et al., 2022).

The residual ambient dose equivalent rate was scored in the entire cavern at 25 successive cool down times, always referring to the end of proton-proton operations before LS3. The time grid is finer close to the end of Run 3: it includes one day after the end of proton-proton operations (for access purposes), one day per week for the first four weeks, and monthly intervals for the first two years. Other cool down times were set to provide estimates after few years of waiting time. FLUKA v4-2.0 (Ahdida et al., 2022; Battistoni et al, 2015; FLUKA.CERN, 2022) hosted by CERN was used for all the simulations.

2.3.2. Results

The simulation of one prompt step and ten different decay scenarios required an extensive computational effort of approximately 730 days of equivalent CPU time. For each scenario, residual ambient dose equivalent maps were plotted for each cool down time provided.

The coordinates system adopted by CMS is a right-handed Cartesian system with the origin placed in correspondence of the interaction point (IP), with the x-axis pointing towards the centre of the LHC ring, the y-axis pointing vertically upwards and the z-axis laying parallel to the beam line. In all the following plots, only one side of the cavern is shown since CMS is symmetric with respect to the plane passing through the IP and perpendicular to the z-

axis. To give a further reference, the experimental cavern floor is a x-z plane at y = -900 cm in all the vertical cuts (Figures 2.5, 2.6, 2.7).

Figure 2.6. CMS "open disk" configuration; residual ambient dose equivalent rate map at 1 month of cool down time after the end of proton-proton operations before LS3

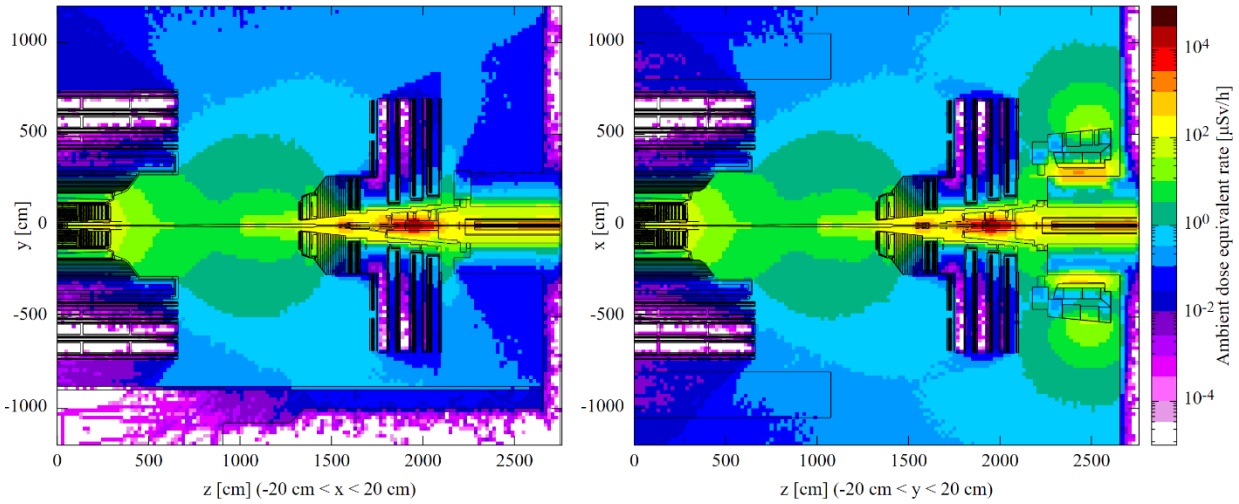

Residual ambient dose equivalent rate maps after 1 month cool down time after the end of proton-proton operations before the beginning of LS3; CMS in "open disk" configuration. Vertical (left) and horizontal (right) cuts of the CMS experimental cavern.

Figure 2.7. CMS "open disk" configuration; residual ambient dose equivalent rate map at 6 months of cool down time after the end of proton-proton operations before LS3

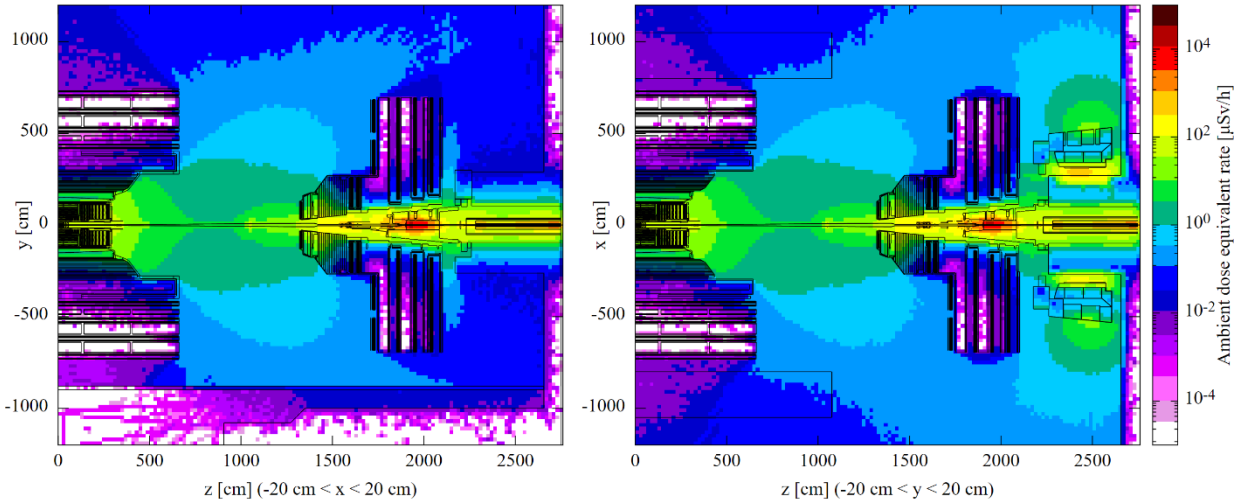

Residual ambient dose equivalent rate maps after 6 months cool down time after the end of proton-proton operations before the beginning of LS3; CMS in "open disk" configuration. Vertical (left) and horizontal (right) cuts of the CMS experimental cavern.

In Figure 2.5, it is possible to observe residual dose rates for CMS in nominal configuration at 1 month cool down time after the end of proton-proton collisions before LS3. In this scenario, the overall radioactivity levels are well below 1 μSv/h in all the accessible areas. The detector itself acts as shielding, and only few weak points can be spotted (z = 1500 cm

and z = 2100 cm close to the beam line). In the beam pipe, some hot spots can be identified where the residual dose rate is greater than 1 mSv/h.

Considering the same cool down time (1 month), the residual ambient dose equivale rate grows when the endcap disk is opened (Figure 2.6). At floor level, the increase is of about a factor of 10. The highly activated components of the inner tracking systems considerably contribute to the residual dose rate levels in the cavern. The movement of the disk, however, allows to shield the hot spot of the so-called VAX region along the beam pipe (z = 2000 cm, x = y = 0 cm). On the horizontal cut, in the region x = ±500 cm, z = 2500 cm, it is possible to see the rotating shielding once opened. This steel-lined, heavy concrete shielding is composed by two quasi semi-cylindrical parts that can be opened with a rotation to expose the beam pipe. It allows the retraction of the endcap disk, and ultimately a fast opening of the whole CMS detector for access to the inner systems during maintenance.

For the same configuration, an overall reduction of the radioactivity levels in the cavern can be appreciated at the longer cool down time of 6 months (Figure 2.7). Evaluating residual dose rates at multiple cooling times allows to provide an effective and quantitative support for dose optimization when the planning of Long Shutdowns interventions is scheduled.

2.4. Summary and Conclusions

Estimating residual ambient dose equivalent rates during Long Shutdowns is a challenging task. Multiple inputs are required in a well-defined and collaborative workflow: large experiments define in advance the work plan and consequently the detector configurations; the LHC Run must be summarized in a realistic irradiation profile, based on the target machine performance and conservative, yet reliable, assumptions. Moreover, the model of the detector has to be accurately implemented as a FLUKA geometry and specific software (FLUKA, SESAME, custom scripts to ensure a sufficient degree of automatization) has to be maintained and possibly developed. Finally, considerable computing resources are necessary to perform big sets of simulations and handle data in reasonable time.

The CMS case study was illustrated. At the time of this writing, ten configurations are currently foreseen for LS3-activities. The set of residual ambient dose equivalent rate maps that was computed will give a first overview of the radioactivity levels present in the cavern over a wide grid of cool down times for each configuration. As a further step ahead, it could be possible to estimate residual dose rates of single components. This would provide CERN RP with useful information to organize other tasks such as transport and storage of dismantled parts.

This kind of study can provide a first indication of the ALARA classification and required approved workflow for the various interventions planned during LS3. As it relies on relevant assumptions regarding the irradiation conditions during future runs, further evaluations should be foreseen closer to LS3, when more details about the LHC machine performance are known.

2.5. Acknowledgements

The authors wish to thank the CMS Radiation Simulation working group for providing the original simulation geometry description of the CMS experimental cavern and detector.

2.6. List of references

Ahdida, C. et al. (2022). “New Capabilities of the FLUKA Multi-Purpose Code”. Frontiers in Physics, Volume 9, 788253

Battistoni, G. et al. (2015) “Overview of the FLUKA code”, Annals of Nuclear Energy 82, 10-18 (2015)

Bozzato, D. et al. (2022) “LHC and HL-LHC luminosity and irradiation profiles for Radiation Protection studies”. CERN internal document, EDMS Document Number 2641646

Brüning, O. and Rossi, L. (2015) *The High Luminosity Large Hadron Collider*. Singapore: WORLD SCIENTIFIC. doi.org/10.1142/9581D.

Cooijmans, T. and Guthoff, M. (2015) *SESAME Documentation*. CERN internal document

Evans, L. and Bryant, P. (2008) “LHC Machine”, *Journal of Instrumentation*, 3(08). doi:10.1088/1748-0221/3/08/S08001.

FLUKA.CERN (2022), *FLUKA*, viewed 11 November 2022, <https://fluka.cern>

Froeschl, R. (2020) *The SESAME and DORIAN codes for residual dose rate calculations*. CERN internal document, EDMS Document Number 2378246

The CMS Collaboration (2008) “The CMS experiment at the CERN LHC”, Journal of Instrumentation, 3(08):S08004-S08004

Vlachoudis, V. (2009) "FLAIR: A Powerful But User Friendly Graphical Interface For FLUKA". Proc. Int. Conf. on Mathematics, Computational Methods & Reactor Physics (M&C 2009), Saratoga Springs, New York

2.7. List of abbreviations and acronyms

CMS	Compact Muon Solenoid
HL-LHC	High Luminosity Large Hadron Collider
IP	Interaction Point
LHC	Large Hadron Collider
LS	Long Shutdown
RP	Radiation Protection

3. Activation calculations of selected RPV internal components for optimal decommissioning of nuclear power plants

Reuven Rachamin[1*], Jörg Konheiser[1], Marcus Seidl[2]
[1] Helmholtz-Zentrum Dresden-Rossendorf, 01328 Dresden, Germany
[2] PreussenElektra GmbH, 30457 Hannover, Germany
[*]r.rachamin@hzdr.de

By the middle of 2023, all German nuclear power plants (NPPs) will have been shut down. The final shutdown is followed by a post-operational phase in which measures can be carried out to prepare for the NPPs dismantling and decommissioning. One of the tasks in preparation for the dismantling is to acquire precise knowledge of the activation of the reactor pressure vessel (RPV) and its internal components. In this study, the specific activities of selected RPV internal components of a German PWR were calculated with a method based on the combined use of two Monte-Carlo codes, MCNP6 and FLUKA2021. In the first step, the MCNP6 code was used to calculate the neutron fluence rate characteristics (spectrum, distribution, and current entering the component' segment surfaces) in the studied component' segment using a 3D detailed reactor model. The neutron fluence rate prediction capability of the MCNP6 model has been validated via metal foil-activation measurements carried out in two German PWRs. The validation studies showed that the MCNP6 model is reliable and suitable for evaluating the neutron radiation field in the reactor for the ensuing activation calculations. In the second step, the FLUKA2021 code was used to calculate the specific activity distribution in the studied component' segment using a 3D exact model of the segment and complex source terms built based on the neutron fluence rate parameters calculated using the MCNP6 code. The results of the calculations were obtained with great accuracy and evidenced that the method used can serve as a powerful and non-destructive tool for the radiological characterization of the RPV and its internals.

3.1. Introduction

In 2011, the German Atomic Energy Act was amended to phase out the use of nuclear energy for the commercial production of electricity. Consequently, all German nuclear power plants (NPPs) will have been permanently shut down by the middle of 2023. After their final shutdown, the NPPs should be decommissioned and dismantled. To dismantle the NPPs in a safe, economical, and timely manner, decommissioning studies have to be performed for each of the shutdown NPPs. The present study focuses on the decommissioning of a German pressurized water reactor (PWR), which is the most common NPP type in Germany.

One important task in decommissioning studies is estimating the neutron activation distribution within the NPP components that have emerged during its lifetime operation. Such knowledge can significantly minimize radioactive waste and contribute to the safety of the operating personnel and the general public. Therefore, this study aimed to precisely estimate the specific activities in the reactor pressure vessel (RPV) and its internal components, which are the most activated parts of the reactor. The activation calculations were performed using a method combining two Monte-Carlo codes, MCNP6 (version 6.2) and FLUKA2021 (version 2021.2.7). The MCNP6 code (Goorley et al., 2012; Werner et al., 2018) was used to calculate the neutron fluence rate parameters in the studied component using a 3D detailed reactor model. The FLUKA2021 code (Ferrari et al., 2005;

Battistoni et al., 2014; Ferrari et al., 2022) was then used to calculate the specific activity distribution in the studied component using a 3D exact model of the component and complex source terms built based on the neutron fluence rate characteristics calculated using the MCNP6 code.

The activation calculations of the RPV and its internals based on the MCNP6-FLUKA2021 codes sequence is the subject of this paper. Section 2 presents the MCNP6 calculations. It gives a brief description of the German PWR model and its validation. Then, it shows the evaluation of the neutron fluence rate characteristics of the studied RPV internal components. Section 3 presents the FLUKA2021 calculations. It describes the studied RPV internal components and verifies the neutron source terms. Finally, it gives the activation calculations of the studied RPV internal components. Section 4 summarizes and concludes the study.

Figure 3.1. MCNP model of a German PWR (in red: activation monitors locations)

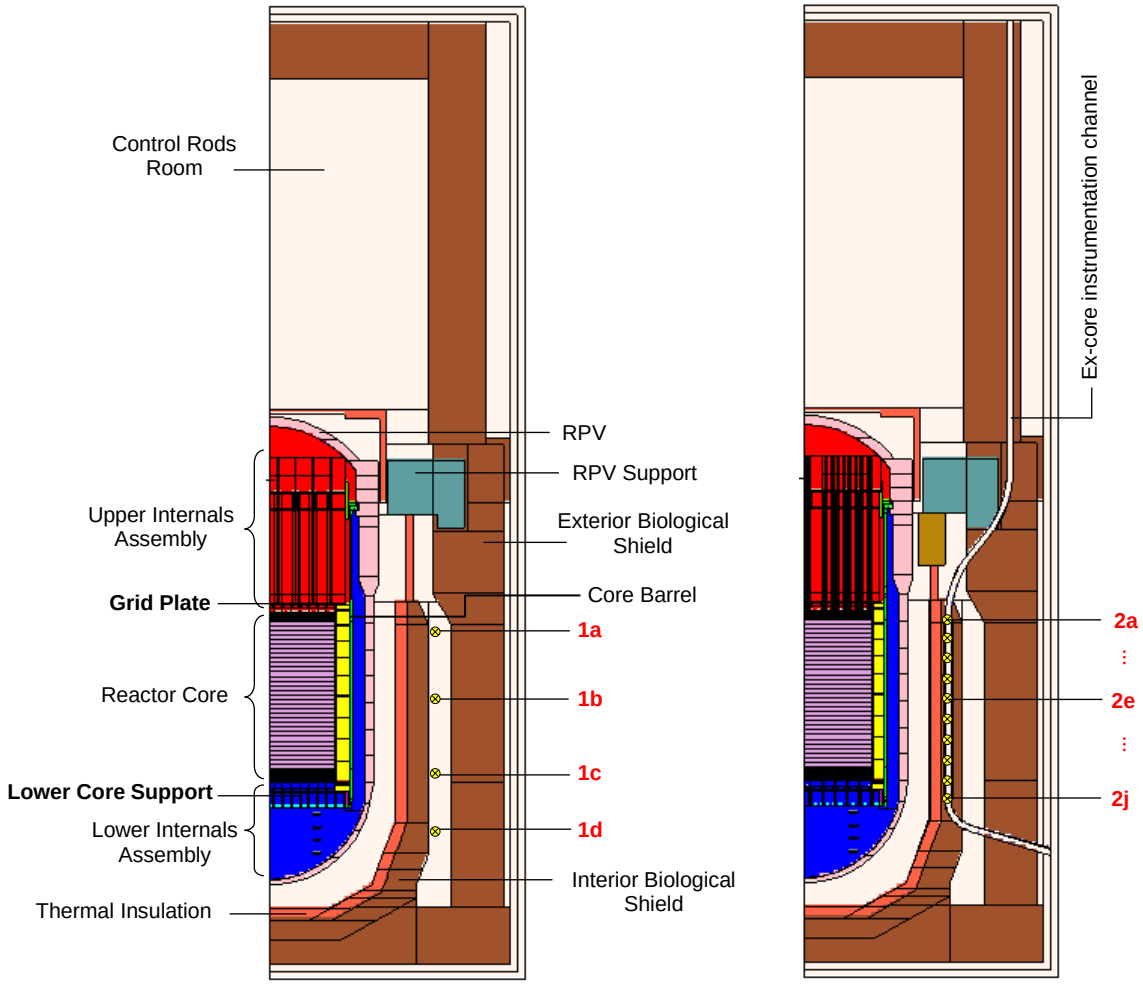

3.2. MCNP Calculations

3.2.1. Reactor model description

The extent and activation levels in an NPP depend on the neutron fluence within its components. Hence, neutron fluence is one of the essential parameters for activation calculations. Therefore, to estimate precisely the neutron fluence distribution within a

German PWR, a detailed 3D model was developed and simulated using the Monte Carlo code MCNP6 (Rachamin et al., 2021; Rachamin et al., 2022). The reactor was modeled in detail based on technical drawings from the studied PWR plants. The material densities and compositions used in the model were based on the available documents from the plants and literature data. A schematic view of the model is shown in Figure 3.1. The simulated model extends from the reactor core through the reactor pressure vessel (RPV) and its internals into the surrounding components, which include the thermal insulation and the interior and exterior biological shields. The lower internals assembly (i.e., the stool, flow distribution plate, lower core plate) and the upper internals assembly (i.e., grid plate, support column, upper core support, top plate), as well as the foot and head regions of the fuel assemblies composing the reactor core, were modeled in detail to represent the ex-vessel neutron leakage accurately. The fuel assemblies' body, i.e., the active core region, was modeled as a homogeneous cell. Up to the outer wall of the exterior biological shield, the reactor exhibits quarter symmetry in the radial direction. Therefore, the model represents only a quarter of the reactor. The neutron source was defined in the active core region of the model as a fixed source. The fixed source was determined and specified in the model as a pin-by-pin distribution, where each pin was divided into 32 axial layers. Such a fine pin-wise specification, especially in the outer core region (i.e., the outer fuel assemblies), is essential to obtain accurate neutron fluence results outside the core.

3.2.2. Validation of the reactor model prediction credibility

Metal foil-activation measurements were carried out to validate the neutron fluence prediction credibility of the developed MCNP6 model (Barkleit et al., 2022; Rachamin et al., 2022). Metal foil-activation measurement has been successfully used in reactor dosimetry for many years. It is an ideal method for collecting information on neutron fluence in an active reactor. When neutrons activate a metal foil, it emits characteristic energy gamma rays, which can be counted and related to the neutron fluence incident on the foil. Therefore, foil activation measurement can provide sufficient information on the neutron fluence needed for validating, tuning, and optimizing the Monte Carlo model.

The measurements took place in two active German PWRs. In one reactor (denoted as reactor No. 1), the activation monitors were placed outside the interior biological shield in different angular positions (monitors 1a-1d). In the second reactor (denoted as reactor No. 2), the activation monitors were placed along one of the empty ex-core instrumentation channels (situated at the angle of 84^{o}), passing through the reactor interior and exterior biological shields (monitors 2a-2j). The locations of the monitors are illustrated in Figure 3.1. Each activation monitor is made of an aluminum box filled with thin metal foils packed in Kapton tape. The metal foils have a thickness of 0.1 mm and a size of 5 x 5 mm to 10 x 10 mm or 10 mm in diameter. Titanium, Iron, Nickel, Copper, Zinc, Indium, and Tin were chosen as the materials for the activation foils. Each of these materials provides information on different neutron energy spectrum ranges (i.e., thermal, epithermal, and fast energy range), giving a complete picture of the energy distribution of the neutron fluence. The activation monitors were placed in the reactors during the annual revision and irradiated for one fuel cycle (approximately one year). After the activation monitors were removed and recovered, the activation of the metal foils was measured with a coaxial high-purity germanium (HPGe) detector (GMX, 30% efficiency, Fa. Ortec-Ametek).

According to the experimental measurements, the neutron fluence and the corresponding activation were calculated within a small sphere (with a radius of 2.5 cm) around each of the monitor's estimated axial locations in the studied reactors. For these calculations, the neutron source was integrated over the irradiation time of the monitors in each reactor. The activation was calculated using the International Reactor Dosimetry and Fusion File

(IRDFF-II) data library (Trkov et al., 2020) for all the metal foil reactions, of which the data is available in the library. For the reactions for which the data is unavailable in the IRDFF-II library, the ENDF/B-VII.1 library (Chadwick et al., 2011) was used instead.

Figure 3.2. Activation calculations (C) vs. experimental measurements (E) for ^{113}In (n,ɣ) ^{114m}In in reactor No. 1

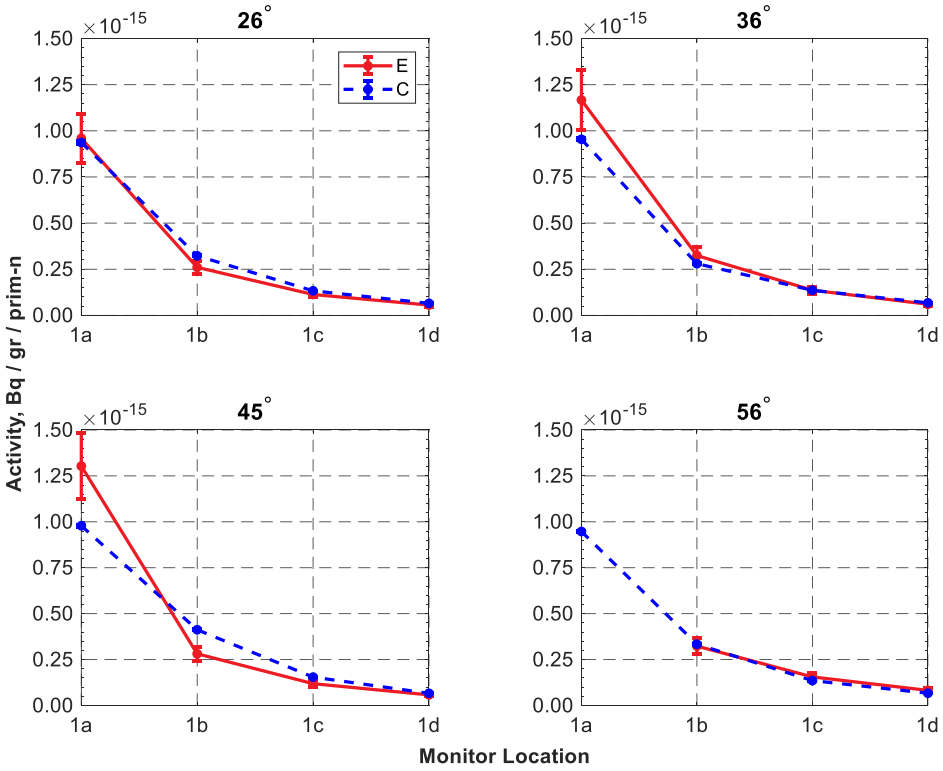

Figure 3.2 and Figure 3.3 present the activation calculations vs. measurements for the ^{113}In (n,ɣ) ^{114m}In reaction. Figure 3.2 shows the results obtained for the monitors placed in angular positions of 26º, 36º, 45º, and 56º outside the interior biological shield of reactor No. 1. As can be noted, a good agreement was obtained between the calculated and measured activities. The C/E ratio (Calculation to Experiment ratio) between the nominal values ranges between 0.75 to 1.46. Figure 3.3 shows the results obtained for the monitors placed along the ex-core instrumentation channel (situated at the angle of 84º) of reactor No. 2. Since the monitors were manually lowered down from the top of the channel, their exact location inside the channel space has some uncertainty (the channel has a diameter of 15 cm). Therefore, the calculations were performed for three possible locations of the monitors: close to the inner wall of the channel (In), in the middle of the channel (Mid.), and close to the outer wall of the channel (Out). As can be noted, a good agreement was obtained between the calculation and the measurement values. The calculation values of the three possible locations lie in the range of the measurement uncertainties.

It should be noted that the agreement between the calculated and measured activities depends on many parameters, such as the geometry approximations and material definitions, the neutron source definitions, the cross-section data realism, the estimated location of the monitors, and the measurement uncertainties. The calculations and the measurement methodology used in this study were optimized to minimize the impact of

these parameters and achieve high-accuracy results. The reactor was modeled in great detail, the most updated cross-section data were used, and high-fidelity simulations and measurements were performed. Therefore, as was obtained for the ^{113}In (n,γ) ^{114m}In reaction presented above, a good agreement was obtained between the calculations and measurements for all the examined metal foils activation reactions.

Figure 3.3. Activation calculations (C) vs. experimental measurements (E) for ^{113}In (n,γ) ^{114m}In in reactor No. 2

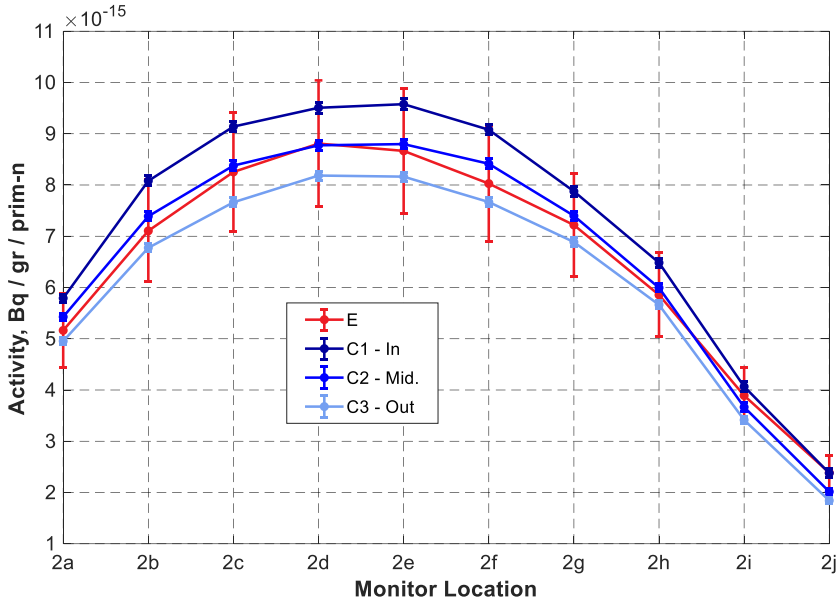

3.2.3. Evaluation of the neutron fluence rate characteristics of the RPV internal components

The validation studies shown above indicate that the MCNP6 model is reliable and suitable for evaluating the neutron radiation field in the RPV and its internal components for the following activation calculations. In this paper, the activations of two components are demonstrated. These components are the grid plate and the lower core support. The grid plate, depicted in Figure 3.4a, has a thickness of 4 cm and is located above the reactor core. The lower core support, shown in Figure 3.4b, has a thickness of about 39 cm and is located below the reactor core. For the analysis, the components were divided into axial layers of 1 cm thickness (4 axial layers for the grid plate and 39 axial layers for the lower core support). Each layer was divided into a mesh of 23x23 cm (fuel assembly size). The fluence rate characteristics were calculated for each (23x23x1) cm segment of the studied component using the developed MCNP6 model. The characteristics include the neutron current entering the segment from each surface (as a function of energy and angle) and the neutron fluence rate distribution in a fine mesh. These data were then used to create the source term for the studied component activation calculations using the FLUKA2021 code. Figure 3.5 presents the neutron fluence distribution in a 23x23 cm mesh obtained for the lowest layer of the grid plate and the top layer of the lower core support, which are the closest layers to the reactor core and, therefore, the most activated. The distribution maps were obtained with maximum relative errors of less than 1%.

Figure 3.4. The grid plate and lower core support models

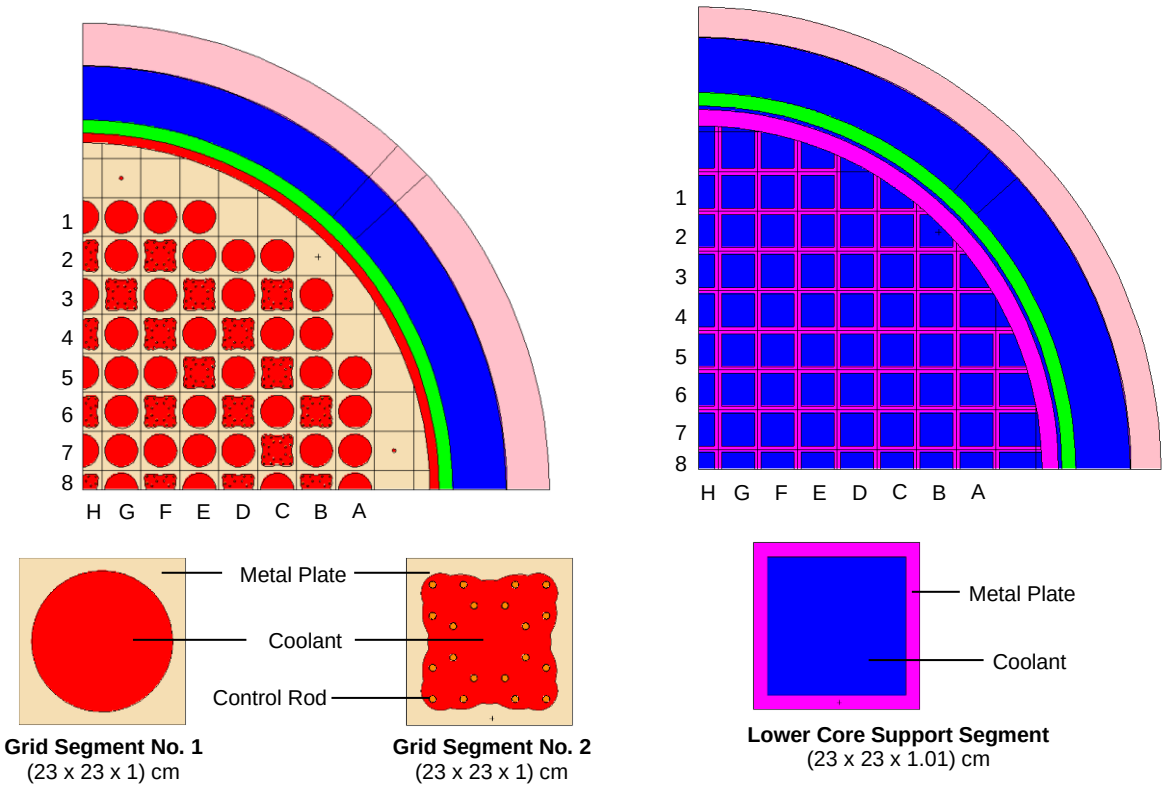

a. Grid plate

b. Lower core support

Figure 3.5. Neutron fluence distribution in the grid plate (lowest layer) and the lower core support (top layer) obtained from the MCNP calculations (reference solution)

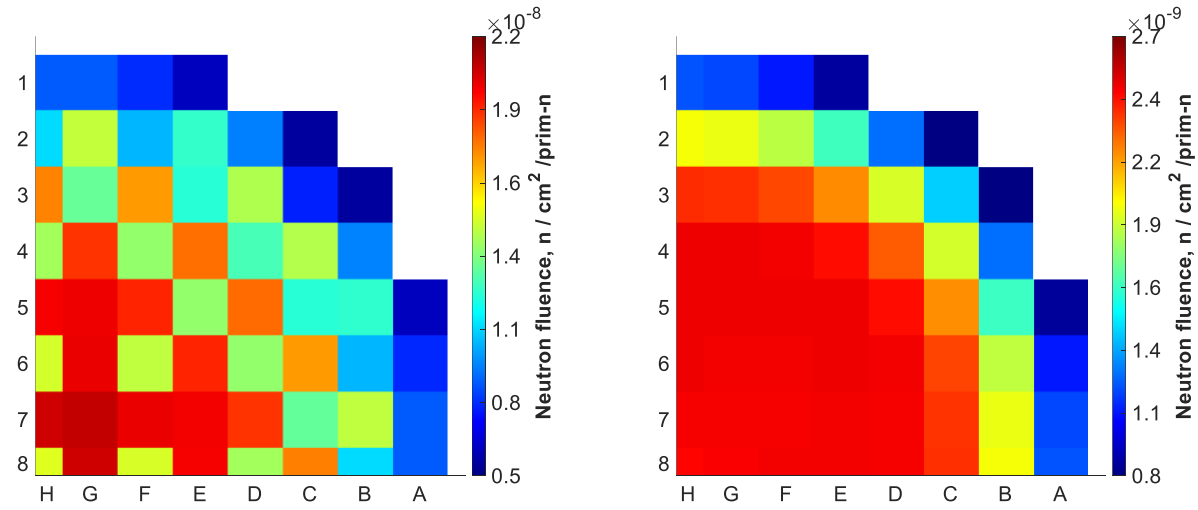

a. Neutron fluence distribution in the lowest layer of the grid plate

b. Neutron fluence distribution in the top layer of the lower core support

3.3. FLUKA calculations

3.3.1. Components model description and source terms verification

As mentioned earlier, the FLUKA2021 activation calculations were performed using a 3D exact model of the studied component segments and complex source terms built based on the neutron fluence rate parameters calculated using the MCNP6 code. The calculations were performed for each segment of the studied component separately. Then, the results were combined to form a full distribution map of the activation in the component. The segment models of the grid plate and lower core support are illustrated in Figure 3.4. To verify that the data for the source terms transferred accurately from the MCNP6 to the FLUKA2021 code, the neutron fluence distribution in each studied component was calculated using the FLUKA2021 code and compared with the MCNP6 reference solution. The FLUKA2021 calculations were performed using its built-in point-wise cross sections library (Sala et al, 2022).

Figure 3.6. Neutron fluence distribution in the grid plate (lowest layer) obtained from the FLUKA calculations and its comparison with the MCNP reference solution (shown in Figure 3.5a)

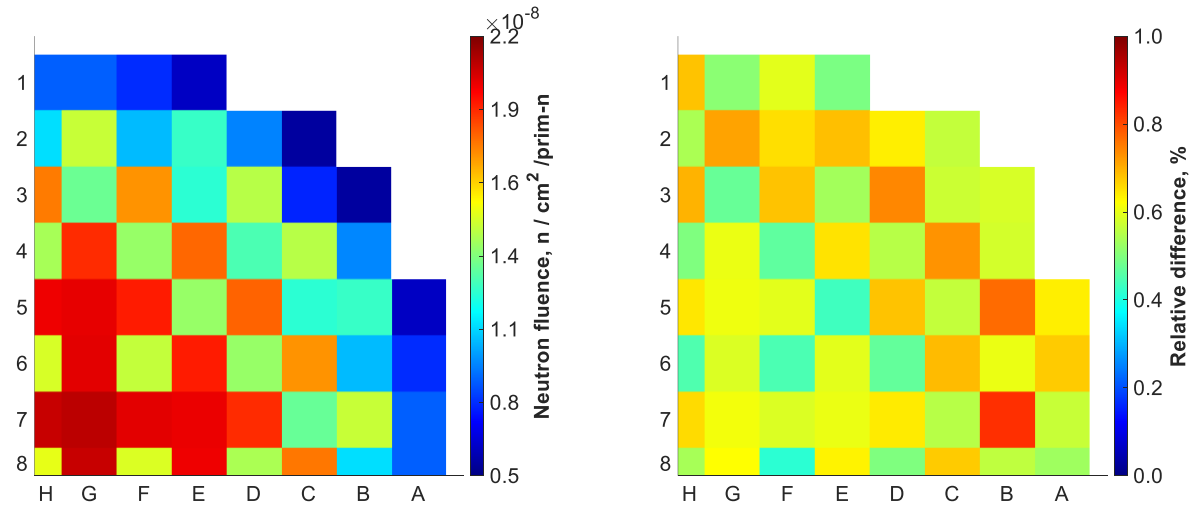

a. Neutron fluence distribution in the lowest layer of the grid plate

b. Relative difference: MCNP vs. FLUKA

Figure 3.6 and Figure 3.7 present the FLUKA2021 results and their comparison with the MCNP6 solutions (shown in Figure 1.5) for the lowest layer of the grid plate and the top layer of the lower core support, respectively. Similar to the MCNP6 results, the distribution maps were obtained from FLUKA2021 with maximum relative errors of less than 1%. As can be noted, for the lowest layer of the grid plate (Figure 3.6), the maximum and average relative differences between the results obtained from the codes are 0.83% and 0.60%, respectively. For the top layer of the lower core support (Figure 3.7), the maximum and average relative differences between the results obtained from the codes are 1.06% and 0.96%, respectively. The same observation was obtained for all the axial layers of the studied components. This indicates that the neutron fluence rate parameters were reliably transferred from the MCNP6 to the FLUKA2021 calculations. Therefore, the FLUKA2021 calculations can be considered a direct continuation of the MCNP calculations.

Figure 3.7. Neutron fluence distribution in the lower core support (top layer) obtained from the FLUKA calculations and its comparison with the MCNP reference solution (shown in Figure 3.5b)

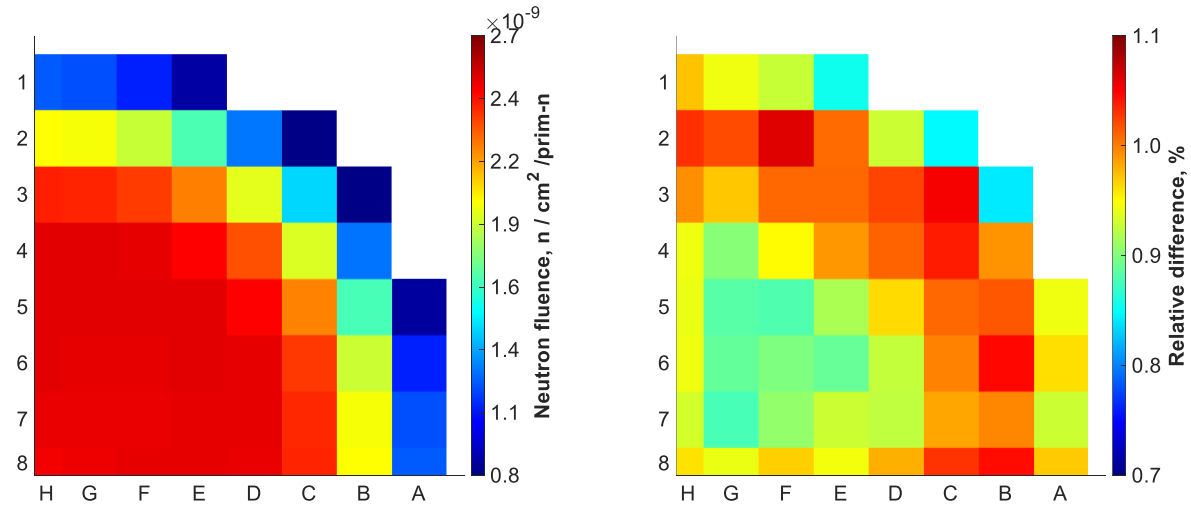

a. Neutron fluence distribution in the top layer of the lower core support

b. Relative difference: MCNP vs. FLUKA

Figure 3.8. Activation distribution in the grid plate (lowest layer) obtained from the FLUKA calculations at the end of life (EOL) and 5y after the EOL

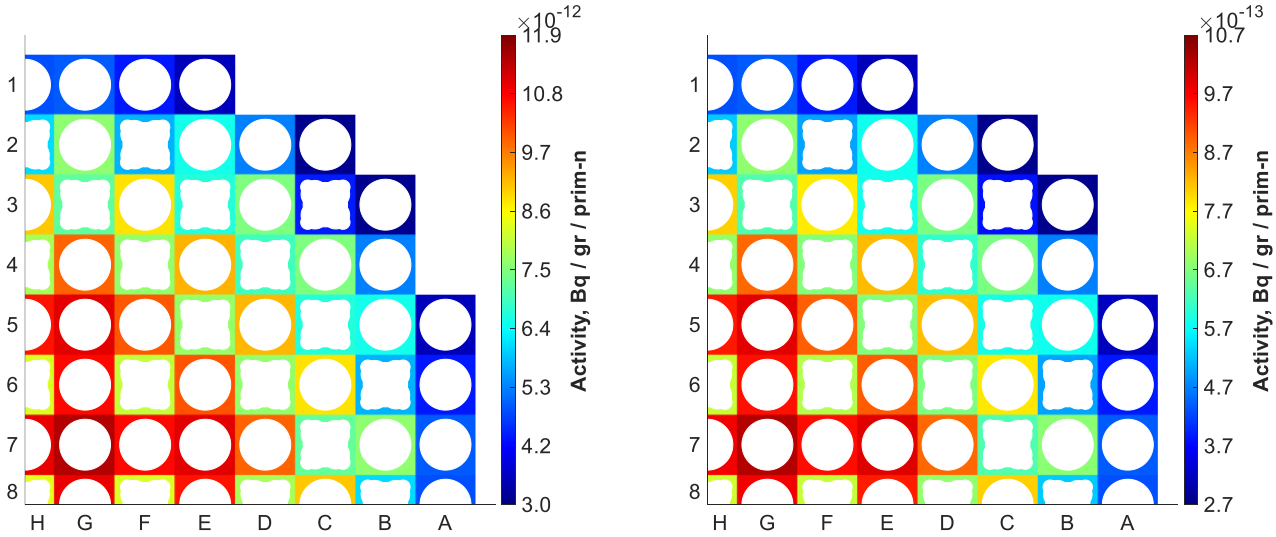

a. EOL

b. EOL + 5y

Figure 3.9. Activation distribution in the lower core support (top layer) obtained from the FLUKA calculations at the end of life (EOL) and 5y after the EOL

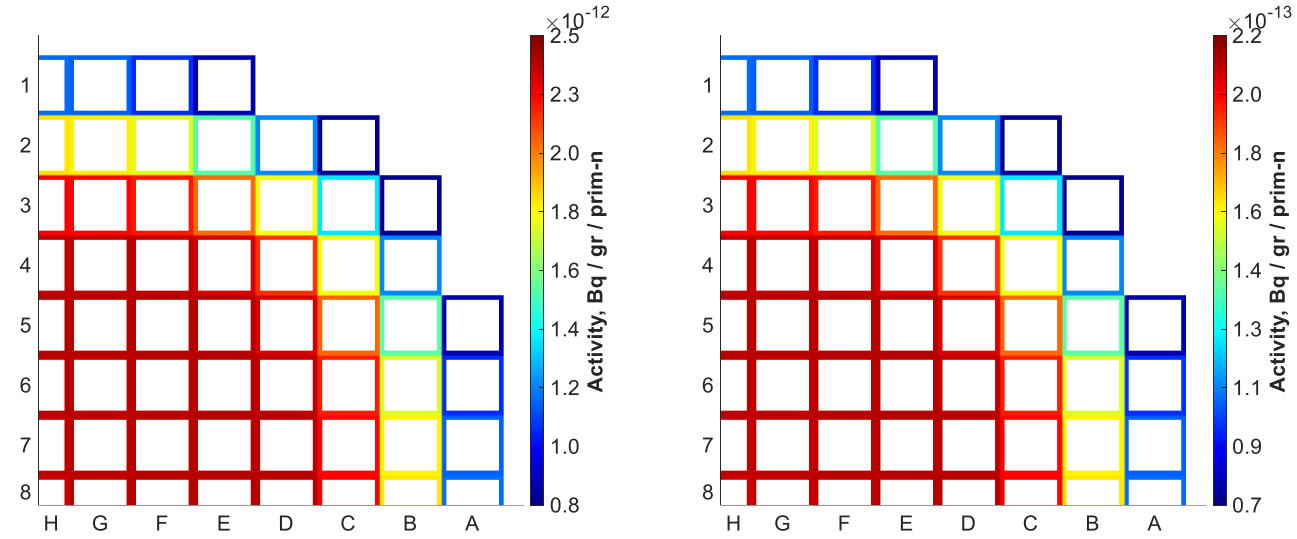

a. EOL

b. EOL + 5y

3.3.1. Activation calculations of selected RPV internal components

The activation calculations were calculated using the FLUKA2021 code, taking into account the reactor's detailed irradiation profile (operating + revision times). Figure 3.8 and Figure 3.9 present the neutron activation distribution within the lowest layer of the grid plate and the top layer of the lower core support that emerged during the reactor's lifetime operation, respectively. As can be noted, after five years of cooling time, the activation level in the studied components drops by about one magnitude with respect to the reactor's EOL. The obtained activation maps can be used as guidelines for planning the studied components' disposal and storage.

3.4. Summary and Conclusions

One of the essential tasks in planning and preparing an NPP for decommissioning is to obtain precise knowledge of the activation levels in its RPV, biological shielding, and other internal components. In that regard, a method based on the combined use of two Monte Carlo codes, MCNP6 and FLUKA2021, was developed to serve as a non-destructive tool for evaluating the activation in an NPP.

This paper presented and demonstrated the novel methodology through the activation calculations of two RPV internal components of a German PWR, Germany's most common NPP type. These components are the grid plate and the lower core support. In the first step, the MCNP6 code was used to calculate the neutron fluence rate characteristics in the studied component using a 3D detailed reactor model. In the second step, the FLUKA2021 code was used to calculate the specific activity distribution in the studied component using a 3D exact model of the component and complex source terms built based on the neutron fluence rate parameters computed using the MCNP6 code. The prediction credibility of the MCNP6 calculations was validated via experimental measurements, which, in turn, verified

the FLUKA2021 calculations. The activation maps for the studied components were obtained with great accuracy and can be used as guidelines for their disposal and storage.

3.5. Acknowledgements

This work was funded by the Federal Ministry of Education and Research (BMBF) under contract number 15S9409A and by the PreussenElektra GmbH project “Activity calculation”.

3.6. List of references

Barkleit A., Rachamin R., Yassin G., Pönitz E., Konheiser J. (2022), “Experimental activation determination in and on components of nuclear power plants and comparison with activity calculations”, Proc. of 19th Radiochemical Conference, Marianske Lazne, Czech Republic.

Battistoni G., et al. (2014), “The FLUKA Code: Developments and Challenges for High Energy and Medical Applications”, Nuclear Data Sheets, **120**, 211.

Chadwick M. B., et al. (2011), “ENDF/B-VII.1 Nuclear Data for Science and Technology: Cross Sections, Covariances, Fission Product Yields and Decay Data”, Nuclear Data Sheets, **112**, 2887-2996.

Ferrari A., Sala P., Fassò A., and Ranft J. (2005), “FLUKA: a multi-particle transport code”, CERN Yellow report 2005-10, 1–406, INFN/TC_05/11, SLAC-R-773.

Ferrari A., et al. (2022), “FLUKA: status and perspectives”, these proceedings.

Goorley T., et al. (2012), “Initial MCNP6 Release Overview”, Nuclear Technology, **180**, 298-315.

Rachamin R., Konheiser J., Barkleit A., and Seidl M. (2021), “Decommissioning Studies of German PWR: Neutron Fluence Calculations and Experimental Measurements”, Proc. of 15th International Symposium “Conditioning of Radioactive Operational & Decommissioning Wastes”, Dresden, Germany.

Rachamin R., Konheiser J., Barkleit A., and Seidl M. (2022), “Dosimetry for Decommissioning of Nuclear Power Plants”, Proc. of ICRS 14/RPSD 2022, Seattle, WA, USA.

Sala P., et al. (2022), “The FLUKA group- and point-wise neutron treatment”, these proceedings.

Trkov A., et al. (2020), “IRDFF-II: A New Neutron Metrology Library”, Nuclear Data Sheets, **163**, 1-108.

Werner C. J., et al. (2018), “MCNP6.2 Release Notes”, Los Alamos National Laboratory, report LA-UR-18-20808

3.7. List of abbreviations and acronyms

PWR	Pressurised water reactor
NPP	Nuclear Power Plant
RPV	Reactor Pressure Vessel

4. Radiation protection studies for new beam dumps at ISOLDE at CERN

Alice Formento[1], Elodie Aubert[1], Ana-Paula Bernardes[1], Alexandre Dorsival[1], Jose Maria Martin Ruiz[1], Stefano Marzari[1], Simon Mataguez[1], Eliseo Perez-Duenas[1], Fabio Pozzi[1], Heinz Vincke[1], Joachim Vollaire[1]

[1]European Organization for Nuclear Research (CERN), Geneva, Switzerland
[*]alice.formento@cern.ch

ISOLDE is a CERN facility dedicated to the production of radioactive ion beams for applications in atomic physics, nuclear astrophysics, fundamental interactions, and life sciences. The 1.4 GeV proton beam from the Proton Synchrotron Booster, with a maximum current of 2 μA, impinges on a thick target kept at high temperature during irradiation. The generated radionuclides diffuse out of the target and are ionized by an ion source. Then, the radioactive nuclei are extracted, and a mass separator is used to select the radionuclides of interest, which are transported to the experimental area via a beam line system.

Around 80% of the primary proton beam does not interact with the target and is intercepted by a beam dump, one for each of the two target stations. The ISOLDE beam dumps are currently operating at their limit in terms of temperature and mechanical stresses. For these reasons, their exchange is currently being studied together with the design of new beam dumps and related shielding to meet future operational needs (higher beam energy, i.e.,2 GeV, and intensity, up to 6 μA) as well as modern radiation protection standards.

Besides the studies for the future dismantling worksite, a detailed radiation protection analysis via the FLUKA.CERN Monte Carlo code is being performed for the new beam dumps and the related facility consolidation. This work covers various RP aspects such as the study of the envelope target configuration for stray radiation and the definition of the radiological area classification. Moreover, the evaluation and optimisation of: shielding requirements (volume, material, cost), material activation, residual dose rate, and atmospheric releases from air activation cannot be neglected.

4.1. Introduction

The Isotopes mass Separator On Line Device (ISOLDE) is a CERN research facility dedicated to the production of a large variety of radioactive ion beams for applications in the fields of nuclear and atomic physics, solid-state physics, material and life sciences (F. Pozzi et al.,2022) (ISOLDE facility displayed in Figure 4.1).

The 2.8 kW proton beam from the Proton Synchrotron Booster (PSB) (energy of 1.4 GeV and maximum current of 2 μA), impinges on a thick target kept at high temperature (up to 2300 °C) during irradiation. The generated radionuclides diffuse out of the target and are ionized by an ion source; then they are extracted via an electrode with an energy up to 60 keV; eventually a mass separator is used to select the radionuclides of interest, which are transported to the experimental area via a beam line system. Several target materials can be employed being depleted uranium carbide (UC_4) used as target material in more than 65% of ISOLDE experiments.

The target can be placed onto two target stations called Front-Ends: the GPS (General-Purpose Separator) Front-End, which is coupled to a bending magnet and an electrostatic switchyard allowing simultaneous extractions of three beams separated according to their mass; and the HRS (High-Resolution Separator) Front-End, which has two bending magnets with an elaborated ion-optical system for higher order corrections providing an improved resolution in mass. Each target station is equipped with a beam dump to absorb

the proton beam not interacting with the target, which amount to a percentage between 60-70%. Recent studies showed that the beam dumps are currently operating at their limit in terms of temperature and mechanical stresses. For these reasons and in the framework of the ISOLDE Beam Dump Replacement Study (IBDRS), their exchange is currently being studied together with the design of new beam dumps and related shielding to meet future operational needs as well to remain compliant with current radiation protection regulations.

Figure 4.1. ISOLDE Facility

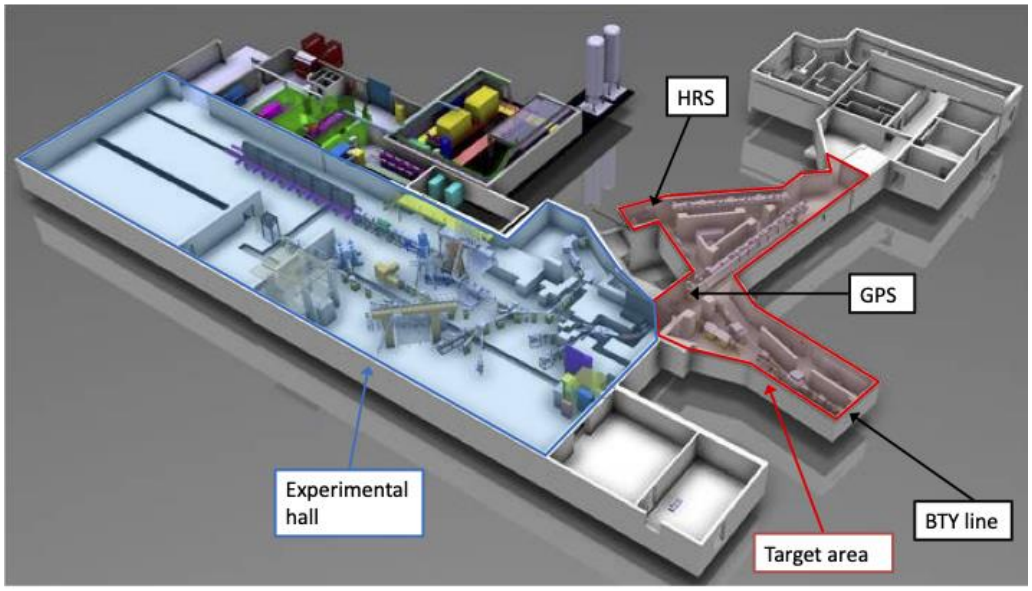

Note: The ISOLDE facility layout, BTY line = beam extraction line from the PSB to ISOLDE
Source: ISOLDE Website: layouts and templates, https://isolde.web.cern.ch/isolde-logos-layouts-and-templates

4.2. IBDRS context and objectives

The ISOLDE beam dumps, installed in the target area during the construction phase of the 4th ISOLDE generation (1991-1992), are passive steel absorbers surrounded by concrete and steel shielding. The target area and the beam dumps are shielded by several metres (up to 8-9 m) of soil, part of which became radioactive. The exchange of the beam dumps will provide several benefits to ISOLDE:

- The new beam dumps and the ancillary equipment, like the dump cooling system, will be designed to cope with an increased proton beam power (up to ~10-20 kW) to profit of the maximum proton energy (2 GeV) and intensity (up to 6 μA) that can be delivered by the PSB.
- The shielding around the target area and the beam dumps will be designed using the new beam parameters, will reduce stray radiation levels in accessible areas well below the applicable limits and will minimize the amount of radioactive soil.
- The unique chance of accessing the surroundings of the target area will open possibilities to consolidate the existing ISOLDE infrastructure in view of ensuring its long-term safe and reliable operation.

The beam dump replacement project can be divided in two major phases:

1. The dismantling phase, which includes the studies and works to perform a safe removal of the present beam dumps and shielding, as well as the preparation of the areas for the installation of the new beam dumps.
2. The consolidation phase, which includes the studies to design and install the new beam dumps, the ancillary equipment, and the new shielding.

Presently, two consolidation concepts are being studied, called BASIC and FLEXI, illustrated in Figure 4.2. BASIC foresees the construction of two shafts (one per beam dump), which will be filled with the required shielding and a service gallery on top of them. If needed the beam dump will be accessible via the service gallery by removing the shielding from the shafts. However, most of the concrete/iron shielding will still be covered by soil and not easily accessible.

The FLEXI concept, which is conceived to be versatile, foresees the design of a new building (not accessible during beam operation); the FLEXI building will be heavily shielded from the target area by concrete, magnetite, and iron blocks. The new building will allow to access the target area shielding and, at a later stage, to integrate further technical and safety improvements, e.g., upgrade of target stations, access to the HRS separator. To ensure that radiation levels outside of the building will remain negligible, the new building will be covered with few metres of soil. In addition, the FLEXI concept will allow a staged approach to the upgrade of the shielding as a function of the evolution of the irradiation parameters. Because of the above-mentioned considerations, the study of the FLEXI concept is currently prioritized.

Figure 4.2. IBDRS concepts

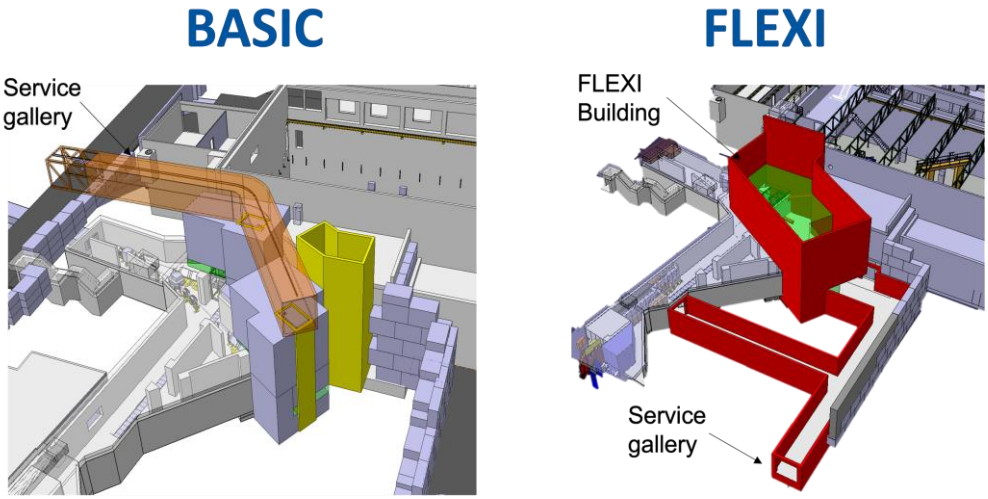

Note: Technical gallery highlighted in orange for the BASIC concept, FLEXI building and technical galleries in red for the FLEXI concepts. In both pictures the soil shielding surrounding the facility is not shown.

4.3. Overview of radiation protection studies

Several radiation protection assessments are being performed for the beam dump replacement study, in particular:

- the assessment of the envelope target configuration for stray radiation simulations;

- the definition of shielding requirements including its optimisation in terms of volumes, material and costs;
- the environmental impact assessment, which includes the contribution of atmospheric releases from the facility (e.g., shot-lived gases from air activation) and of skyshine radiation;
- the analysis of the residual activation inside the target area in case of maintenance interventions and related mitigation measures to optimize the personnel exposure;
- the investigation of the residual radioactivity in the soil surrounding the facility.

These aspects are studied combining the return of experience of thirty years of ISOLDE operation, results from dedicated experimental measurement campaigns and regular RP surveys, and analysis carried out by means of Monte Carlo simulations with the FLUKA[1] code hosted by CERN (C. Ahdida et al, 2022; G. Battistoni et al, 2015, FLUKA Website). The next chapter will focus on the main challenges encountered for the stray radiation simulations for the FLEXI concept.

4.4. FLUKA simulations and related challenges

4.4.1. FLUKA input parameters

FLUKA simulations were performed not only to design the FLEXI concept but also for the present model of the facility to prepare the dismantling phase and to benchmark the geometry modelled in FLUKA against the results of dedicated radiation measurements.

The FLEXI concept was integrated into the existing FLUKA model of the ISOLDE complex; the model shown in Figure 4.3 is the result of several iterations performed to optimize the design of the facility including its shielding. Figure 4.4 and Figure 4.5 show the top view at the beam level and the side view of the shielding implemented towards the GPS beam dump, respectively. Different shielding layers are visible, which account for about 170 m^3 of iron, 230 m^3 of concrete and 390 m^3 of magnetite. The FLEXI building is covered by 3-4 metres of earth; this additional shielding allows to reduce the neutron prompt radiation outside the building and the resulting skyshine radiation.

The shielding calculations for the FLEXI concept were performed assuming a 2 GeV proton beam with a maximum current of 6 μA (or 3.75e13 p/s) corresponding to a beam power of 12 kW. The proton beam impinges onto two targets placed in series:

1. The first target is a 20 cm long, 1.5 cm diameter UC_4 target (3.5 g/cm^3);
2. The second target, which benefit of the non-interacting protons[2], is a 10 cm long and 5 cm diameter higher density UC_4 target (7 g/cm^3).

Although this is a target configuration never employed before at ISOLDE, it was chosen as sufficiently conservative to account for potential future operational needs. The simulations for the present model of the facility were performed using the present irradiation parameters, i.e., 1.4 GeV beam energy and 2 μA beam current with one single UC_4 target (same target parameters as the first target for the FLEXI concept).

[1] FLUKA v4-2.2

[2] This is principle on which the construction of the MEDICIS facility is based on (with a ref to https://doi.org/10.3389/fmed.2021.693682)

Figure 4.3. FLEXI building in FLUKA

FLEXI building geometry

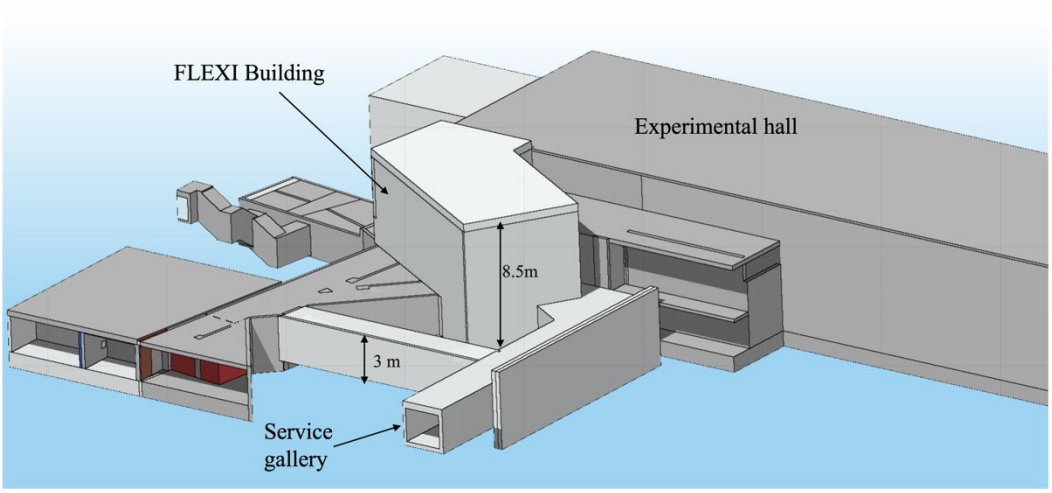

Shielding inside the FLEXI building

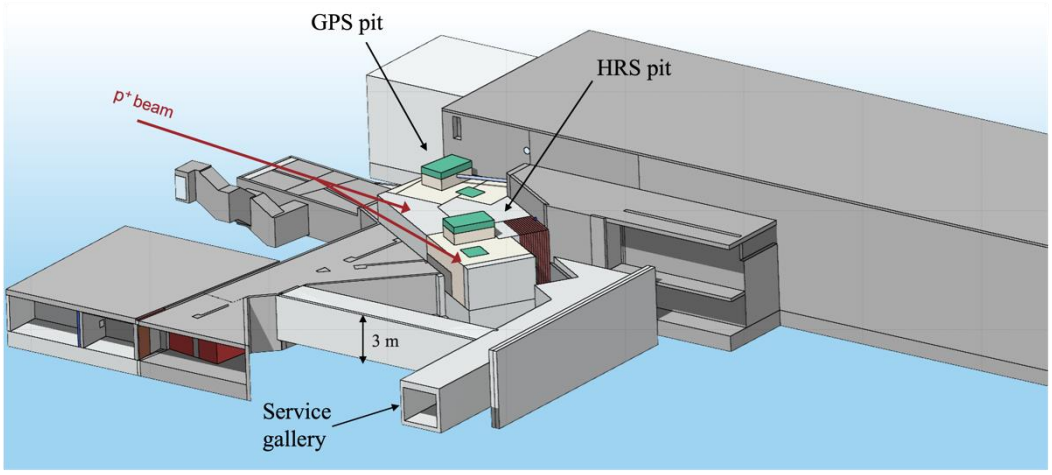

Note: In both pictures the soil covering the facility is not shown. Concrete shielding is represented in grey, iron in green and a light yellow is used for magnetite.

Figure 4.4. FLEXI shielding top view (beam level)

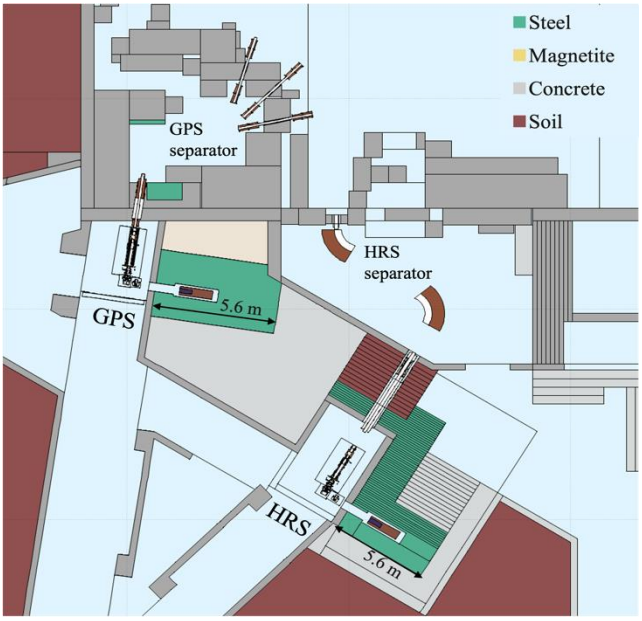

Figure 4.5. HRS shielding lateral view

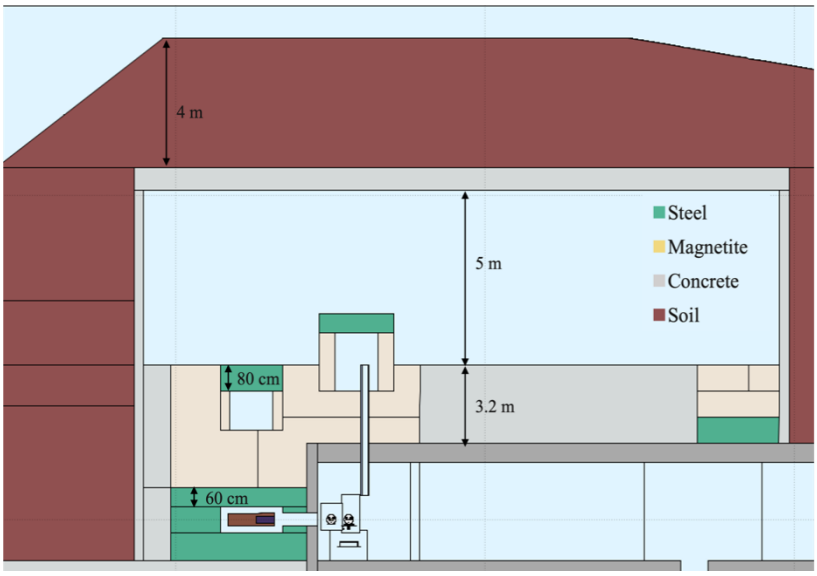

Table 4.1. Proprieties of the target materials

Target material	UC_4	UCx high density
Density	3.5 g/cm^3	7 g/cm^3
Radius	0.75 cm	2.5 cm
Length	19.6 cm	10 cm
Volume	~35 cm^3	~196 cm^3
Mass	~121 g	~1374 g
Composition [weight percentage]	U-238: 82.99% U-235: 0.23% C-12: 16.78%	

4.4.2. Multiple simulations and iterations

One of the complexities of this study is performing Monte Carlo simulations for several irradiation scenarios (two target stations, two consolidation concepts, several potential target combinations), therefore it is of utmost importance to optimise the number of configurations to be studied. For instance, the feedback from operational experience (stray radiation measurements) coupled with simplified Monte Carlo simulations contributed to reducing the number of target combinations to be evaluated for shielding calculations. In addition, a reliable version control, as well as a collaborative working environment was ensured to follow-up the frequent updates of the Monte Carlo studies by employing GitLab, a web-based Git repository.

4.4.3. Thick shielding problem

In a thick Monte Carlo shielding problem, the probability of a particle to reach a specific region outside the shielding can be very low and therefore the statistical uncertainty very high. To overcome this issue but still maintaining an acceptable computational time, one could profit of biasing techniques, which are widely available in the Monte Carlo codes. The aim of a biasing technique is to maintain a uniform population compensating for attenuation, e.g., due to distance or absorption. For the FLUKA simulations described in this paper, two biasing techniques were employed.

- **Region-based importance biasing:** This is achieved in FLUKA by means of the BIASING input card and it is applied when a particle crosses a region boundary. An importance factor is assigned by the user to each region and the relative importance R of two adjacent regions is calculated:
  - if a particle moves toward a higher importance region (R > 1) a surface splitting algorithm is performed: a certain number of particle replicas, proportional to R, are created and the total weight of all replicas is equal to the weight of the original particle.
  - if a particle moves toward a lower importance region (R < 1) a Russian Roulette algorithm is applied: the survival probability of the particle is proportional to R and the weight of all surviving particles is equal to the weight of all incoming particles.

  This technique could require changes in geometry to properly assign importance coefficients and it might turn not to be the most efficient choice in areas with complicated region organisation/division or that, in a process of optimisation, are subject to frequent changes or updates.
- **Material-based importance biasing:** This is achieved in FLUKA by programming a user-defined routine, called usimbs.f (User define Importance

BiaSing). The routine is called at every particle step and it allows to implement importance biasing scheme based on region number and/or phase space coordinates. For ISOLDE-related simulations, the regions were grouped per material type (e.g., concrete, iron, magnetite) and an exponential law of attenuation was assumed to calculate the corresponding importance ratio R. The routine is very powerful but time-consuming since it is called at every particle step. Therefore, the user must balance the time gained by biasing with that employed by calls.

Figure 4.6. Material-based importance biasing: usimbs.f

```
61
62 *    The exact region number will depend on the input file
63 *    This checks if the particle is not a neutron (JTRACK == 8)
64      IF (JTRACK .NE. 8) THEN
65         FIMP = 1.0D0
66         RETURN
67 *    Starting regions that does not requeire biasing
68      ELSE IF ( MREG .LT. 1 ) THEN
69         FIMP = 1.0D0
70         RETURN
71 *    Iron biasing
72      ELSE IF ( (MREG .GE. 1 .AND. MREG .LE. 64)
73     &       .OR. (NEWREG .GE. 1 .AND. NEWREG .LE. 64) ) THEN
74         WIDTH = 23.0D0
75 *    Magnetite biasing
76      ELSE IF ( (MREG .GE. 95 .AND. MREG .LE. 98)
77     &        .OR. (NEWREG .GE. 95 .AND. NEWREG .LE. 98) ) THEN
78         WIDTH = 25.0D0
79 *    Concrete biasing
80      ELSE IF ( (MREG .GE. 146 .AND. MREG .LE. 236)
81     &        .OR. (NEWREG .GE. 146 .AND. NEWREG .LE. 236) ) THEN
82         WIDTH = 59.0D0
83 *    Soil biasing
84      ELSE IF ( (MREG .GE. 335 .AND. MREG .LE. 349)
85     &       .OR. (NEWREG .GE. 335 .AND. NEWREG .LE. 349) ) THEN
86         WIDTH = 76.0D0
87      ELSE
88         FIMP = 1.0D0
89         RETURN
90      END IF
```

Note: Screenshot of part of the usimbs.f; being MREG starting region, NREG final region, WIDTH attenuation length for the material, FIMP importance ratio between the position at the end and at the beginning of the step
Source: CERN 2022, FLUKA, User define Importance BiaSing

4.4.4. Consolidation of existing facility

Consolidating an existing facility, as it is the case for ISOLDE, can be very complex since constraints in terms of available space for additional shielding (in addition to its cost) shall be considered. By optimising the shielding materials, it is possible to achieve the required radiation levels and to overcome space limitations. For instance, dedicated radiation protection studies have shown that magnetite can be a considered a valuable compromise between the better shielding properties of iron for high-energy neutrons with respect to the lower cost of concrete Magnetite can also be produced in a range of different densities and can be mixed with other composite to modify the shielding/absorption properties (e.g., with colemanite, which, thanks to its boron content, can absorb low-energy neutrons).

4.4.5. Validation of the FLUKA model

For relatively old facilities information on geometry and materials employed might be scarce and/or incomplete; this affects the accuracy of the Monte Carlo geometrical model and the results. A good practice is to perform visual inspection and geometrical measurements. When this is not possible, e.g., not accessible areas, a benchmark against radiation measurements can be used to renormalize the results of the Monte Carlo simulations.

For this reason, stray radiation measurements were carried out around the ISOLDE complex: several positions were investigated using fixed radiation monitors (high-pressurized hydrogen-filled ionisation chambers) as well as commercial extended-range neutron rem-counters (WENDI-II and LUPIN) (WENDI-II detector, G. Manessi, (2013).

As an example, the so-called RILIS (Resonance Ionization Laser Ion Source) room in the ISOLDE experimental hall was investigated. The RILIS room is classified as Simple Controlled Radiation Area (ambient dose equivalent rate, H*(10), limit of 50 μSv/h if its occupancy is lower than 20% of the working time); it is used by ISOLDE personnel to tune the lasers to enhance the production of specific radioactive ion beams.

The results of FLUKA simulations (Figure 4.8) show a dose rate exceeding the limit of 50 μSv/h for the present model (1.4 GeV and 2 μA) and exceeding 300 μSv/h for the FLEXI model (2 GeV and 6 μA).

The radiation measurements performed in this area showed dose rate up to ~20 μSv/h and therefore still compliant with the radiological area classification. The discrepancy with the Monte Carlo results can be explained by the limited accuracy of the simulated geometrical model. Visual inspections in this area cannot be performed due to the inaccessibility and the limited amount of available information is not sufficient for an accurate modelling of the shielding.

However, the results of the FLUKA simulations for this room can be renormalized using stray radiation measurements; this will provide a more realistic estimate of the ambient dose equivalent rates in case of energy and intensity upgrade.

Figure 4.7. FLUKA geometry for RILIS area

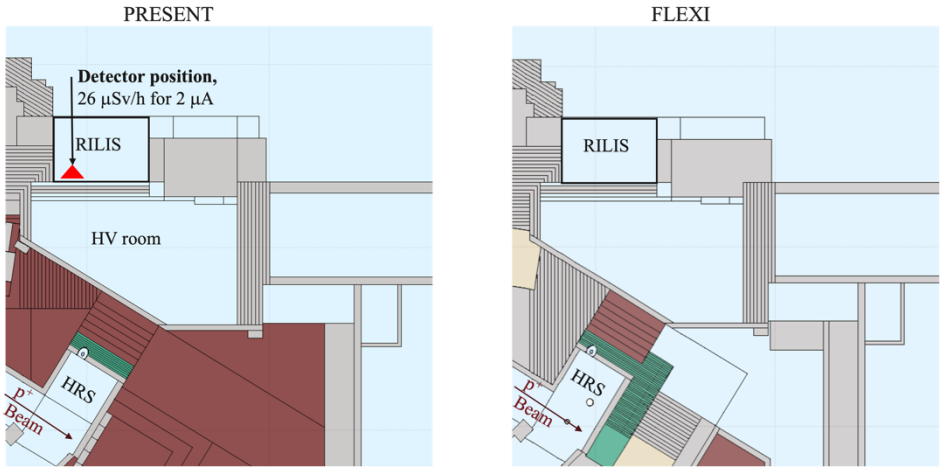

Figure 4.8. Prompt dose rate simulations for RILIS area

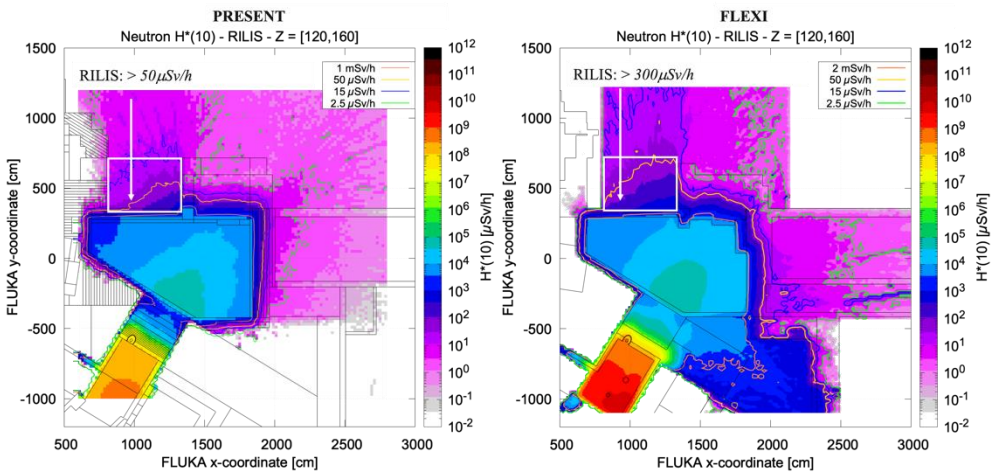

Note: Ḣ*(10) results in Sv/h, on the left Present ISOLDE (1.4GeV, 2μA, one target), on the right FLEXI (2GeV, 6μA, two target station).

4.5. Conclusions: summary and future aspects

Several RP evaluations are being carried out to study the replacement of the present ISOLDE beam dumps and to consolidate the ISOLDE complex in view of a potential beam energy and intensity upgrade. The present paper provides an overlook on the main challenges encountered during the shielding design phase together with solutions and ideas for improvements. The comprehensive RP study that is being conducted will allow to safely exploit the maximum capacities of ISOLDE and to guarantee its reliable operation for the next decades.

4.6. List of references

F. Pozzi (CERN) et al., Operational Radiation Protection Challenges at MEDICIS, a CERN Facility for the Production of Non-Conventional Isotopes for Medical Research, ICRS 14/RPSD 2022, Seattle WA, (2022), Pages 207-210

A.-P. Bernardes et al., ISOLDE beam dump replacement study project plan and work packages description, EDMS 2469313 v.1.0 (2021)

FLUKA.CERN, Website: https://fluka.cern

C. Ahdida, D. Bozzato, D. Calzolari, F. Cerutti, N. Charitonidis, A. Cimmino, A. Coronetti, G. L. D'Alessandro, A. Donadon Servelle, L. S. Esposito, R. Froeschl, R. García Alía, A. Gerbershagen, S. Gilardoni, D. Horváth, G. Hugo, A. Infantino, V. Kouskoura, A. Lechner, B. Lefebvre, G. Lerner, M. Magistris, A. Manousos, G. Moryc, F. Ogallar Ruiz, F. Pozzi, D. Prelipcean, S. Roesler, R. Rossi, M. Sabaté Gilarte, F. Salvat Pujol, P. Schoofs, V. Stránský, C. Theis, A. Tsinganis, R. Versaci, V. Vlachoudis, A. Waets, M. Widorski, *"New Capabilities of the FLUKA Multi-Purpose Code"*, Frontiers in Physics 9, 788253 (2022).

G. Battistoni, T. Boehlen, F. Cerutti, P.W. Chin, L.S. Esposito, A. Fassò, A. Ferrari, A. Lechner, A. Empl, A. Mairani, A. Mereghetti, P. Garcia Ortega, J. Ranft, S. Roesler, P.R. Sala, V. Vlachoudis, G. Smirnov, *"Overview of the FLUKA code"*, Annals of Nuclear Energy 82, 10-18 (2015).

V.Vlachoudis, *"FLAIR: A Powerful But User Friendly Graphical Interface For FLUKA"*, in Proc. Int. Conf. on Mathematics, Computational Methods & Reactor Physics (M&C 2009), Saratoga Springs, New York, 2009.

AP.Bernardes, J.Vollaire, E.Perez-Duenas, JM.Martin Ruiz, S.Marzari, F.Pozzi, G.Dumont, R.Mouret, JP.Rodary, S.Mataguez, *Presentations at the IBDRS Project Management Board* - 17.05.2022 EDMS ISL-PM-PP-0005 v.1

T. E. Booth, J. S. Hendricks, *"Importance estimation in forward Monte Carlo calculations"* Nucl. Technol./Fusion, 5, 90-100 (1984).

WENDI-II detector https://www.thermofisher.com/order/catalog/product/FHT762WENDI2

G. Manessi, M. Silari, C. Welsch, M. Caresana, M. Ferrarini, (2013). The lupin detector: Supporting least intrusive beam monitoring technique through neutron detection. IBIC 2013: Proceedings of the 2nd International Beam Instrumentation Conference.

4.7. List of abbreviations and acronyms

CERN	Conseil Européen pour la Recherche Nucléaire (Europe)
ISOLDE	Isotope Separator On Line Device
PSB	Proton Synchrotron Booster
IBDRS	ISOLDE Beam Dump Replacement Study
RP	Radiation Protection
ALARA	As low as reasonably achievable
RILIS	Resonance Ionization Laser Ion Source

5. Activation benchmarking of metals by 9.6 GeV electrons at PAL-XFEL

Nam-Suk Jung[1], **Mahdi Bakhtiari**[2], **UkJae Lee**[1], **Hee Hoon Kim**[1], **Hee-Seock Lee**[1]
[1] Pohang Accelerator Laboratory / POSTECH
[2] Division of Advanced Nuclear Enginnering / POSTECH
Corresponding Author(s): nsjung@postech.ac.kr

In our previous work [1], samples of low carbon steel, stainless steel, aluminum and copper were irradiated in the stray radiation field results from the 9.6 GeV electron beam hitting a thick copper target at the PAL-XFEL main beam dump bunker. The induced activity concentration in the samples were measured using gamma-ray spectroscopy and were compared with the old version of FLUKA, 2011.2x. In this work, we used the latest versions of the Monte Carlo codes FLUKA 4-2.2 (CERN branch) and PHIS-3.28/DCHAIN-SP-3.23 for benchmarking. The measured and the calculated induced activities in the samples will be discussed.

References

[1] N.S. Jung et al., in 5th International Workshop on Accelerator Radiation Induced Activation (ARIA19), September 23-25, Daejeon, Korea

6. Radiation transport calculations supporting the ISIS muon colli mator replacement project

Steven Lilley
ISIS neutron and muon source, STFC, Rutherford Appleton Laboratory Didcot, UK
Corresponding Author(s): steven.lilley@stfc.ac.uk

The ISIS spallation and muon facility uses a proton beam accelerated to 800 MeV in a linac and synchrotron to generate neutrons and, via an intermediate carbon target, muons. The muon inte mediate target is located on the extracted proton beam before the neutron spallation target on ISIS target station one. After the muon target there are a series of collimators followed by quadrupole magnets to shape the proton beam before the neutron target.

In 2020 the ISIS muon collimator 1 had a small leak in an area which had previously been repaired, the decision was made to replace the muon collimator. This paper details the radiation transport simulations performed both for the calculation of the induced activity in the collimator as a result of the proton beam interactions and the shielding design of the flasks to enable the safe removal of the highly active muon collimator.

The induced activity calculations were performed using FLUKA [1,2], this was chosen due to the ability to perform proton and neutron transport, activation and decay dose rates calculation in a single simulation.

The shielding flask design calculations were made using MCNP [3] based on the decay photon source term calculated using FLUKA. There were several flasks designed for the different high dose rate components including a steel inner layer into which the most active component was winched before it could be removed from the area and placed within its final shielded storage cask.

The MCNP simulations utilised global variance reduction using the FWCADIS method built into Advantg [4] to generate weight windows in order to achieve low variance around all sides of the casks.

MCNP simulations were also performed to investigate the shielding design of the collimator and its surrounding shielding, to determine if there were any improvements and if the dose rates during proton beam operations would be acceptable within the ISIS target station one hall.

The results of the simulations are compared against the health physics measurements taken as the collimator was removed. The agreement is very good given the differences in cooling times between the planned and actual removal times, the uncertainties the irradiation history of the collimator due to varying beam conditions over its lifetime and the material composition uncertainties.

[1] "The FLUKA Code: Developments and Challenges for High Energy and Medical Applications" T.T. Böhlen, F. Cerutti, M.P.W. Chin, A. Fassò, A. Ferrari, P.G. Ortega, A. Mairani, P.R. Sala, G. Smirnov and V. Vlachoudis,, Nuclear Data Sheets 120, 211-214 (2014)

[2] "FLUKA: a multi-particle transport code" A. Ferrari, P.R. Sala, A. Fasso', and J. Ranft, CERN-2005-10 (2005), INFN/TC_05/11, SLAC-R-773

[3] MCNP6 User's Manual, Version 1.0, LA-CP-13-00614, Los Alamos National Laboratory, 2013.

[4] ADVANTG—An Automated Variance Reduction Parameter Generator, ORNL/TM-2013/416 S. Mosher et al. 2013